

The Interaction of Two Unsteady Point Vortex Sources in a Deformation Field in 2D Incompressible Flows

Armand Vic^{1*}, Xavier Carton^{1**}, and Jonathan Gula^{1,2***}

¹*Univ. Brest, CNRS, Ifremer, IRD,
Laboratoire d’Océanographie Physique et Spatiale (LOPS), IUEM,
29280 Plouzané, France*

²*Institut Universitaire de France (IUF),
75005 Paris, France*

Received August 31, 2021; revised October 06, 2021; accepted October 29, 2021

Abstract—Taking into account the coupling of the ocean with the atmosphere is essential to properly describe vortex dynamics in the ocean. The forcing of a circular eddy with the relative wind stress curl leads to an Ekman pumping with a nonzero area integral. This in turn creates a source or a sink in the eddy. We revisit the two point vortex-source interaction, now coupled with an unsteady wind, leading to a time-varying circulation and source strength. Firstly, we recover the various fixed points of the two vortex-source system, and we calculate their stability. Then we show the effect of a weak amplitude, subharmonic, or harmonic time variation of the wind, leading to a similar variation of the circulation and the source strength of the vortex sources. We use a multiple time scale expansion of the variables to calculate the long time variation of these vortex trajectories around neutral fixed points. We study the amplitude equation and obtain its solution. We compute numerically the unstable evolution of the vortex sources when the source and circulation have a finite periodic variation. We also assess the influence of this time variation on the dispersion of a passive tracer near these vortex sources.

MSC2010 numbers: 34D20

DOI: 10.1134/S1560354721060034

Keywords: wind oceanic vortex interaction, vortex-source dynamics, system of ODE, equilibrium point and stability, multiple time scale expansion, dispersion of passive tracers

1. INTRODUCTION

Vortices are essential features in ocean dynamics [5, 6]. They are ubiquitous at least at the ocean surface [8] and they contribute substantially to the meridional heat and momentum transfer. Large oceanic vortices have a moderate Rossby number (the ratio between the Coriolis parameter and the inertial accelerations) and a finite Burger number (which measures the relative influences of global rotation and of fluid stratification). Such vortices have been accurately studied using the quasi-geostrophic (QG) model. In particular, the stability of isolated QG-vortices, and QG-vortex interactions have been investigated, see [7, 9, 10, 17–20, 23, 24]. The simplest vortex interaction occurs between pointwise structures. Point vortex interaction has also been the subject of many studies investigating, in particular, the onset of Hamiltonian chaos [2, 11–15, 25]).

Recent studies of oceanic vortices have shown the importance of taking into account the oceanic flow in the atmospheric forcing terms for a proper evaluation of the strength and durability of these vortices [21]. Also, the Gulf Stream latitude of detachment from the coast and its eastward extent have been proved to be sensitive to a wind forcing properly taking into account the presence of vortices [22].

* E-mail: armand.vic@univ-brest.fr

** E-mail: xcarton@univ-brest.fr

*** E-mail: jonathan.gula@univ-brest.fr

In the present study, we explore the consequence of taking into account the relative wind stress on a vortex. We show that a source/sink flow component appears in the vortex flow. We analyze the interaction of two identical point vortex sources (or vortex sinks) in an external deformation flow mimicking the influence of neighbouring vortices. The motion of point-vortex sources has already been addressed in previous studies [3, 4]. The first paper lists the integral invariants of the problem and the cases of integrability of the equations. It then describes the motion of two point vortex sources. The second paper lists the fixed points of two vortex sources in a deformation flow and briefly addresses the case of a time-varying deformation flow.

In Section 2, we complement these studies by considering that, due to the interaction of the wind with the vortex sources, both the source strength and the vortex circulation vary periodically in time. In Section 3, we look at the dynamical system and compute the equilibrium points and their stability. In Section 4, we follow the method of [15], a multiple time expansion, to obtain an amplitude equation for the slow time variation of the position of each vortex source and we study this amplitude equation with respect to this time variation of the vortex source and circulation. Finally, we model numerically the evolution of the two point vortex sources and of passive particles moving around them in Section 5. Conclusions, perspectives and physical interpretations are finally provided in the last section.

2. MODELLING THE RELATIVE ATMOSPHERIC FORCING OF A VORTEX FLOW

2.1. Basic Equations

The linearized momentum equations on the f -plane for an ocean, forced by a wind stress $\vec{\tau}$, are

$$\begin{cases} \partial_t u - f_0 v = (-1/\rho_0) \partial_x p + (\tau_x/\rho_0) - ku \\ \partial_t v + f_0 u = (-1/\rho_0) \partial_y p + (\tau_y/\rho_0) - kv, \end{cases} \tag{2.1}$$

where k is a friction coefficient (a necessary loss of energy of this ocean to balance the momentum input by the wind).

For low frequency, low Rossby number motions, we neglect the relative acceleration and replace the pressure gradient by a geostrophic velocity:

$$\begin{cases} -f_0 v &= -f_0 v_g + (\tau_x/\rho_0) - ku \\ f_0 u &= f_0 u_g + (\tau_y/\rho_0) - kv. \end{cases} \tag{2.2}$$

Using the subscript ‘‘a’’ for the ageostrophic velocity $u_a = u - u_g$, we have

$$\begin{cases} -f_0 v_a + ku &= (\tau_x/\rho_0) \\ f_0 u_a + kv &= (\tau_y/\rho_0). \end{cases} \tag{2.3}$$

Taking the curl of the system (2.3), we obtain

$$f_0 \vec{\nabla} \cdot \vec{u}_a + k \vec{z} \cdot \vec{\nabla} \times \vec{u} = \vec{z} \cdot \vec{\nabla} \times \vec{\tau} / \rho_0. \tag{2.4}$$

Thus, we see that the wind stress curl $\vec{\tau}$ can have an influence on both the vorticity $\omega = \nabla \times u$ and the velocity divergence $\nabla \cdot u$ (the source-sink term). In particular, if the wind has a steady or a time-varying component, it will induce steady or time-varying velocity divergence and curl. This source-sink effect is next explained in more detail.

2.2. The Relative wind Stress Curl

Recent work [21] has shown that, for the ocean mesoscales, and in particular for the dynamics of oceanic vortices, the wind stress should be computed using the relative velocity of the air to the ocean:

$$\vec{\tau} = \rho_{\text{air}} C_D |\vec{u}_{\text{air}} - \vec{u}_{\text{ocean}}| (\vec{u}_{\text{air}} - \vec{u}_{\text{ocean}}) \tag{2.5}$$

(hereafter referred to as relative wind stress) rather than the total wind velocity

$$\vec{\tau}_a = \rho_{\text{air}} C_D |\vec{u}_{\text{air}}| \vec{u}_{\text{air}} \tag{2.6}$$

(the absolute wind stress). In these expressions, ρ_{air} is the density of the air, C_D is the drag coefficient (about $1.5 \cdot 10^{-3}$ for $|\vec{u}_{\text{air}}| = 15$ m/s), \vec{u}_{air} is the wind velocity, and \vec{u}_{ocean} is the velocity of the oceanic currents.

In what follows, we estimate the difference induced by taking the relative rather than the absolute wind stress, using a simple configuration:

- a zonal and horizontally sheared wind $\vec{u}_{\text{air}} = (U_0 - qy)\vec{i}$.
- a circular vortex oceanic flow $\vec{u}_{\text{ocean}} = \Upsilon r \vec{e}_\theta$ for $0 < r < R$ (we neglect the vortex deformation due to the wind, in this simple estimate), where \vec{e}_θ is the tangential vector to the circle, R is the vortex radius and Υ (capital upsilon) is the vortex rotation rate.

From there, we can compute the relative wind stress through

$$\vec{u}_{\text{air}} - \vec{u}_{\text{ocean}} = \begin{pmatrix} U_0 - qy + \Upsilon r \sin(\theta) \\ -\Upsilon r \cos(\theta) \end{pmatrix} = U_0 \begin{pmatrix} 1 + \frac{\Upsilon - q}{U_0} y \\ -\frac{\Upsilon}{U_0} x \end{pmatrix}, \quad (2.7)$$

so

$$|\vec{u}_{\text{air}} - \vec{u}_{\text{ocean}}| = U_0 \sqrt{\left(1 + \frac{\Upsilon - q}{U_0} y\right)^2 + \frac{\Upsilon^2}{U_0^2} x^2}. \quad (2.8)$$

We next assume that $qR/U_0 \sim \Upsilon R/U_0 \sim \varepsilon$ (in practice on the order of 10^{-2}). Setting

$$\varepsilon\alpha = \frac{\Upsilon - q}{U_0} y, \quad \varepsilon\gamma = \frac{\Upsilon}{U_0} x, \quad (2.9)$$

we find via a Taylor expansion that

$$\vec{\tau} = \tau_0 \begin{pmatrix} 1 + 2\varepsilon\alpha + \varepsilon^2(\alpha^2 + \frac{\gamma^2}{2}) \\ -\varepsilon\gamma - \varepsilon^2\alpha\gamma \end{pmatrix}, \quad (2.10)$$

where $\tau_0 = \rho_{\text{air}} C_D U_0^2$.

The wind stress curl is evaluated at orders 0, ε , ε^2 . The first two orders give

$$\nabla \times \begin{pmatrix} \tau_0 \\ 0 \end{pmatrix} = 0, \quad \nabla \times \begin{pmatrix} 2\varepsilon\alpha \\ -\varepsilon\gamma \end{pmatrix} = -\tau_0 \frac{2q + \Upsilon}{U_0}. \quad (2.11)$$

The effect of the atmosphere-ocean coupling becomes apparent. In the absence of wind shear ($q = 0$), the curl of τ at order ε^1 would be null for an absolute wind stress.

The presence of a wind stress curl leads to an Ekman vertical velocity (Ekman pumping):

$$w_E = \frac{1}{\rho_o} \nabla \times \frac{\vec{\tau}}{f_0}, \quad (2.12)$$

where ρ_o is the seawater density.

It should be noted that, from this expression, one can compare the effect of the relative wind stress to the effect of the Earth's curvature on the Ekman vertical velocity. The former is

$$w_E(\text{air} - \text{ocean}) = -\frac{\rho_{\text{air}}}{\rho_{\text{ocean}}} C_D U_0 \frac{\Upsilon + 2q}{f_0}, \quad (2.13)$$

while the latter is

$$w_E(\beta) = -\beta \frac{\rho_{\text{air}}}{\rho_{\text{ocean}}} C_D \frac{U_0^2}{f_0^2}. \quad (2.14)$$

Using $\Upsilon \sim q \sim 10^{-5} \text{s}^{-1}$ and $U_0 = 15$ m/s, one obtains that the Ekman vertical velocity due to the absolute wind stress is about 30% of the one due to the relative wind stress.

2.3. Ekman Pumping and Point Vortex Sources

We next calculate the source/sink magnitude S_0 associated with the Ekman vertical velocity. To compute the order of magnitude, we assume here that the source/sink term S_0 and the circulation of the vortex Γ_0 are decorrelated. Assuming that the Ekman pumping is uniform over the vortex area, we can calculate the order of magnitude for $S_0 = S\pi R^2 w_E$.

We can also compare the radial velocity thus created, $v_R = S_0/(2\pi RH)$, to the vortex velocity $v_\theta = \Upsilon R$. With $R = 15$ km, the radial velocity is of the order of $2.25 \cdot 10^{-3}$ m/s, while the azimuthal velocity is $v_\theta = 0.15$ m/s. The source/sink magnitude S_0 is therefore about 1.5% that of the circulation Γ_0 .

Note that such vortices are not identical to vortices in a stratified ocean with free density interfaces. Such vortices, in a steady circular configuration, would have no vertical velocity.

Hereafter we assume that the vortex sources are point vortex sources. This is a strong assumption which would, in practice, suppress the effect of the wind stress curl. In fact, this point-vortex assumption means that we only study the vortex motion and not its deformation.

3. INTERACTION OF TWO POINT VORTEX SOURCES

The study of this interaction proceeds in two steps. Firstly, we consider a steady wind and so constant circulation Γ_0 and source/sink magnitude S_0 . Secondly, we consider a time-oscillating circulation $\Gamma(t)$ and address the vortex motion via a multiple time scale method.

3.1. Equations of Motion

We consider two similar vortex sources in the plane (see Fig. 1) on which an external deformation flow acts. This external flow mimicks the effect of surrounding vortices or currents. This problem is analytically tractable, in particular, if we assume central symmetry. Using this symmetry, we derive the equations for only one of the two vortex sources. Vortex source 1 has polar coordinates (r, θ) and, by symmetry, the second vortex source has $(r, \theta + \pi)$.

Vortex-source 1 is submitted to the influence of:

- vortex-source 2:

$$\begin{cases} \dot{r} = \frac{S_0}{2\pi(2r)}, \\ r\dot{\theta} = \frac{\Gamma_0}{2\pi(2r)} \end{cases} \quad (3.1)$$

- the external deformation flow composed of a global rotation and a strain:

$$\begin{cases} \dot{r} = rA \cos(2\theta), \\ r\dot{\theta} = r\Omega - rA \sin(2\theta). \end{cases} \quad (3.2)$$

The vortex-source motion is therefore governed by

$$\begin{cases} \dot{r} = \frac{S_0}{4\pi r} + rA \cos(2\theta), \\ \dot{\theta} = \frac{\Gamma_0}{4\pi r^2} + \Omega - A \sin(2\theta). \end{cases} \quad (3.3)$$

All the physical parameters $(S_0, \Gamma_0, \Omega, A)$ are assumed to be nonzero.

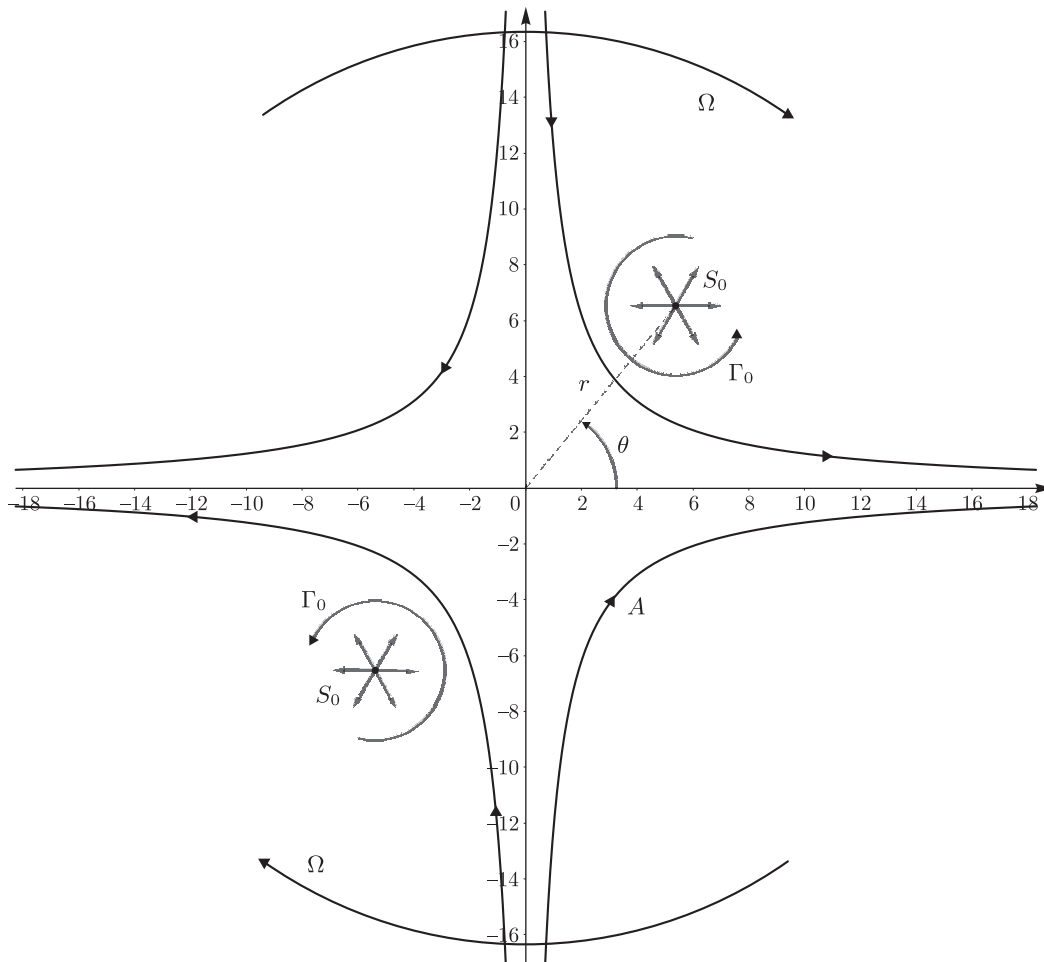


Fig. 1. The two similar point vortex sources in a deformation flow.

3.2. Equilibrium Points and Stability

3.2.1. Preliminaries

The equilibrium points $(r_0, \theta_0) \in \mathbf{R}_+^* \times [-\frac{\pi}{4}, \frac{3\pi}{4}[$ satisfy:

$$\begin{cases} \frac{S_0}{4\pi r_0} + r_0 A \cos(2\theta_0) = 0, \\ \frac{\Gamma_0}{4\pi r_0^2} + \Omega - A \sin(2\theta_0) = 0. \end{cases} \tag{3.4}$$

Let (r_0, θ_0) be an equilibrium. To determine its stability, we calculate the Jacobian matrix $D_{(r_0, \theta_0)} \mathbf{u}$ from the velocity field:

$$\mathbf{u}(r, \theta) = \begin{pmatrix} \frac{S_0}{4\pi r} + r A \cos(2\theta) \\ \frac{\Gamma_0}{4\pi r^2} + \Omega - A \sin(2\theta) \end{pmatrix}, \tag{3.5}$$

$$D_{(r_0, \theta_0)} \mathbf{u} = \begin{pmatrix} -\frac{S_0}{2\pi r_0^2} & \frac{-\Gamma_0}{2\pi r_0} - 2r_0 \Omega \\ \frac{-\Gamma_0}{2\pi r_0^3} & \frac{S_0}{2\pi r_0^2} \end{pmatrix}. \tag{3.6}$$

Its characteristic polynomial is

$$\chi(X) = X^2 - \frac{S_0^2 + \Gamma_0^2 + 4\pi r_0^2 \Gamma_0 \Omega}{4\pi^2 r_0^4}. \tag{3.7}$$

Depending on the sign of

$$\Delta_0 = S_0^2 + \Gamma_0^2 + 4\pi r_0^2 \Gamma_0 \Omega, \tag{3.8}$$

we have a neutral (or center) equilibrium point (if $\Delta_0 < 0$) or a saddle equilibrium point if $\Delta_0 > 0$.

Since saddle points are unstable, and since we wish to describe the long-term evolution of the weakly perturbed vortex-source system (see the following section), we only consider neutral equilibria. A necessary condition for the existence of a center then appears:

$$\Gamma_0 \Omega < 0. \tag{3.9}$$

(if $\Gamma_0 \Omega > 0$, the vortices diverge to infinity along the x or y axis). Hereafter, we assume that this condition is satisfied (unless otherwise stated).

Remark 1. Considering the oceanic case, where $S_0 \ll \Gamma_0$, the condition on Δ_0 for the existence of a center becomes approximately $\Gamma_0^2 + 4\pi r_0^2 \Gamma_0 \Omega < 0$.

3.2.2. Existence of a neutral equilibrium point

First, we calculate the position of the equilibria from the system (3.4):

$$\begin{cases} r_0^2 A \cos(2\theta_0) = -\frac{S_0}{4\pi}, \\ r_0^2 A \sin(2\theta_0) = \frac{\Gamma_0}{4\pi} + r_0^2 \Omega \end{cases} \tag{3.10}$$

implies $\tan(2\theta_0) = -\frac{\Gamma_0 + 4\pi r_0^2 \Omega}{S_0}$. Because the function $]-\frac{\pi}{2}, \frac{\pi}{2}[\rightarrow \mathbf{R}, x \mapsto \tan(2x)$ is not injective, we cannot decide analytically (using this method of analysing necessary conditions) if we have

$$\theta_0 = -\frac{1}{2} \arctan \left[\frac{\Gamma_0 + 4\pi r_0^2 \Omega}{S_0} \right], \tag{3.11}$$

or

$$\theta_0 = -\frac{1}{2} \arctan \left[\frac{\Gamma_0 + 4\pi r_0^2 \Omega}{S_0} \right] + \frac{\pi}{2}. \tag{3.12}$$

But this is not a numerical difficulty since the equilibrium points are clear in a streamfunction plot.

Squaring and summing the two equations in (3.10) gives a biquadratic equation in r_0

$$r_0^4 (\Omega^2 - A^2) + \frac{\Gamma_0 \Omega}{2\pi} r_0^2 + \frac{S_0^2 + \Gamma_0^2}{16\pi^2} = 0. \tag{3.13}$$

From this equation, several equilibria can be found (they are detailed in Appendix A). The only equilibrium point which is a center is determined by

$$r_0 = \sqrt{\frac{-\Gamma_0 \Omega + \sqrt{\Delta'}}{4\pi (\Omega^2 - A^2)}} \quad \text{and} \quad \theta_0 = \frac{1}{2} \arctan \left[\frac{\Gamma_0 A^2 - \Omega \sqrt{\Delta'}}{S_0 (\Omega^2 - A^2)} \right] \left(+\frac{\pi}{2} \right), \tag{3.14}$$

where $\Delta' = A^2 (S_0^2 + \Gamma_0^2) - S_0^2 \Omega^2 = S_0^2 (A^2 - \Omega^2) + A^2 \Gamma_0^2$ and where the additional $+\frac{\pi}{2}$ depends on the sign of S_0 . This is valid under the conditions

$$A^2 < \Omega^2 < A^2 \left(1 + \frac{\Gamma_0^2}{S_0^2} \right) \quad \text{and} \quad \Gamma_0 \Omega < 0. \tag{3.15}$$

Remark 2. These conditions do not depend on the sign of S_0 . This will allow us to choose S_0 as a source or a sink with the same intensity.

The various equilibria and their nature depending on the four physical parameters are shown in Fig. 2. This figure shows the presence of an attractive or a repulsive center at the origin of the plane when the source flow is strong (this equilibrium will not be considered further because it corresponds to the final position of the two vortex sources after a merging event). Two saddle points exist when the source flow is weak and when the strain flow is strong. Finally, two centers appear for weak external flow and weak source intensity, and when conditions (3.15) are satisfied.

Remark 3. With $\Gamma_0 < 0, S_0 < 0, \Omega > A > 0$, the oceanographic limit $|S_0| \ll |\Gamma_0|$ leads to the following approximation for the center position: $\theta_0 \approx \pi/4, r_0 \approx \sqrt{-\Gamma_0/[4\pi(\Omega - A)]}$. Note that, though S_0 is not infinitesimal in Fig. 2, the orientation of the centers corresponds to this solution in the upper left case.

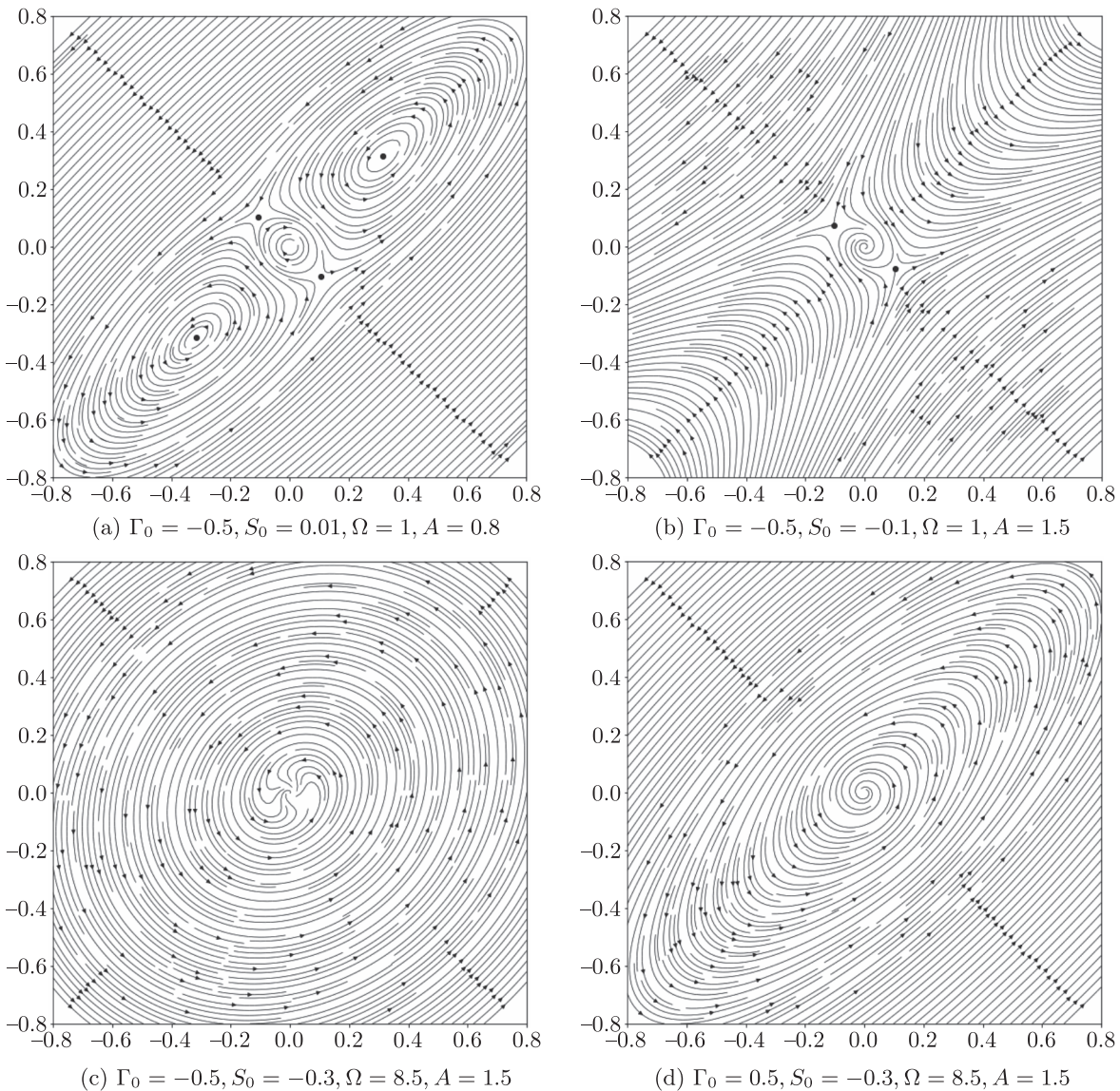


Fig. 2. Vortex-source trajectories for different sets of physical parameter values. Neutral equilibrium points (centers) appear only in the configuration where conditions (3.15) are fulfilled (see the upper left panel). The upper right panel shows a case with a strong strain field; the lower two cases have fast global rotation with either like-signed or opposite-signed circulation and source intensity.

4. VORTEX MOTION WITH UNSTEADY CIRCULATION AND SOURCE-SINK MAGNITUDE

This section is devoted to the motion of a source-sink pair with a periodic circulation and source magnitude, due to the effect of an equally periodic wind stress. This wind stress is assumed to have a dominant steady component and a weak periodic component. In this section, we first address the case of a subharmonic time variation of Γ and of S with respect to the period of rotation of a vortex source around the neutral equilibrium point.

4.1. Weakly Nonlinear Evolution of the Vortex Pair Displaced from a Center with a Subharmonic Variation of Circulation and Source

We consider a center point defined by Eq. (3.14) that we slightly perturb from its equilibrium position. Computed from Eq. (3.7), the natural pulsation of the motion around this center is

$$\omega_0 = \frac{\sqrt{-[S_0^2 + \Gamma_0^2 + 4\pi r_0^2 \Gamma_0 \Omega]}}{2\pi r_0^2}. \tag{4.1}$$

4.1.1. Multiple time scale development

In this subsection, we assume that the wind stress leads to a subharmonic variation of system (3.3) with circulation and source-sink magnitude:

$$\begin{cases} \Gamma(t) = \Gamma_0 (1 + \varepsilon^2 \delta \cos(2\omega_0 t)), \\ S(t) = S_0 (1 + \varepsilon^2 \delta \cos(2\omega_0 t)). \end{cases} \tag{4.2}$$

The algebra for this subharmonic case is detailed here and in Appendix B. To simplify notations, we introduce the constants

$$\begin{cases} a = \frac{S_0}{2\pi r_0^2} = -2A \cos(2\theta_0), \\ b = 2 \left(\Omega + \frac{\Gamma_0}{4\pi r_0^2} \right) = 2A \sin(2\theta_0), \\ c = \frac{\Gamma_0}{2\pi r_0^2} \end{cases} \tag{4.3}$$

such that $a^2 + bc = -\omega_0^2$.

Remark 4. For an oceanic point vortex source, $|S_0| \sim 1.5\%|\Gamma_0|$, so $a \ll b$ and $a \ll c$. Although this is not done here, we could use this to make approximations in the following computations. In Appendix B, we can see that the quotient rates a/b and a/c appear frequently.

The equation of motion is expanded at higher order in ε than in the previous section. Close to (r_0, θ_0) , we expand in ε the time $t = t_0 + \varepsilon t_1 + \varepsilon^2 t_2 + \varepsilon^3 t_3$ and the dynamical variables:

$$\begin{cases} r = r_0 + \varepsilon r_1 + \varepsilon^2 r_2 + \varepsilon^3 r_3, \\ \theta = \theta_0 + \varepsilon \theta_1 + \varepsilon^2 \theta_2 + \varepsilon^3 \theta_3. \end{cases} \tag{4.4}$$

Once substituted in the equation of motion (3.3), we obtain:

- Equations for r :

$$\begin{aligned} \partial_t r &= \varepsilon (\partial_{t_0} r_1) + \varepsilon^2 (\partial_{t_0} r_2 + \partial_{t_1} r_1) + \varepsilon^3 (\partial_{t_0} r_3 + \partial_{t_1} r_2 + \partial_{t_2} r_1) \\ &= \underbrace{\frac{S_0}{4\pi r_0} + A r_0 \cos(2\theta_0)}_{=0} + \varepsilon [-a r_1 - b (r_0 \theta_1)] \end{aligned} \tag{4.5}$$

$$+ \varepsilon^2 \left[-ar_2 - b(r_0\theta_2) + \frac{a\delta r_0}{2} \cos(2\omega_0 t_0) + \frac{a}{2r_0} r_1^2 + \frac{a}{r_0} (r_0\theta_1)^2 - \frac{b}{r_0} r_1 (r_0\theta_1) \right] \quad (4.6)$$

$$+ \varepsilon^3 \left[-ar_3 - b(r_0\theta_3) + \frac{a}{r_0} r_1 r_2 - \frac{ar_1^3}{2r_0^2} - \frac{a\delta}{2} r_1 \cos(2\omega_0 t_0) - a\delta r_0 \omega_0 t_1 \sin(2\omega_0 t_0) \right. \\ \left. - \frac{b}{r_0} (r_2 (r_0\theta_1) + r_1 (r_0\theta_2)) + \frac{a}{r_0^2} r_1 (r_0\theta_1)^2 + \frac{2a}{r_0} (r_0\theta_1) (r_0\theta_2) + \frac{2b}{3r_0^2} (r_0\theta_1)^3 \right] \quad (4.7)$$

• Equations for θ :

$$\partial_t (r_0\theta) = \varepsilon [\partial_{t_0} (r_0\theta_1)] + \varepsilon^2 [\partial_{t_0} (r_0\theta_2) + \partial_{t_1} (r_0\theta_1)] \\ = \underbrace{\frac{\Gamma_0}{4\pi r_0} + r_0\Omega - Ar_0 \sin(2\theta_0)}_{=0} + \varepsilon [-cr_1 + a(r_0\theta_1)] \quad (4.8)$$

$$+ \varepsilon^2 \left[-cr_2 + a(r_0\theta_2) + \frac{c\delta r_0}{2} \cos(2\omega_0 t_0) + \frac{3c}{2r_0} r_1^2 + \frac{b}{r_0} (r_0\theta_1)^2 \right] \quad (4.9)$$

$$+ \varepsilon^3 \left[-cr_3 + a(r_0\theta_3) - c\delta r_1 \cos(2\omega_0 t_0) + \frac{3c}{r_0} r_1 r_2 + \frac{2b}{r_0} (r_0\theta_1)(r_0\theta_2) \right. \\ \left. - \frac{2c}{r_0^2} r_1^3 - \frac{2a}{3r_0^2} (r_0\theta_1)^3 - c\delta r_0 \omega_0 t_1 \sin(2\omega_0 t_0) \right]. \quad (4.10)$$

By gathering terms at each order, we obtain:

At order ε^1 . As expected, we recover from Eqs. (4.5) and (4.8) the unforced harmonic oscillator (the forcing appears only at order ε^2).

$$\begin{cases} \partial_{t_0} r_1 = -ar_1 - b(r_0\theta_1), \\ \partial_{t_0} (r_0\theta_1) = -cr_1 + a(r_0\theta_1) \end{cases} \quad (4.11)$$

with the solution

$$r_1 = C_{1,1}(t_2, t_3) e^{i\omega_0 t_0} + \overline{C_{1,1}}(t_2, t_3) e^{-i\omega_0 t_0}. \quad (4.12)$$

Hereafter, the second term is denoted c.c for “complex conjugate”.

$$r_0\theta_1 = D_{1,1}(t_2, t_3) e^{i\omega_0 t_0} + \text{c.c.}, \quad (4.13)$$

with

$$D_{1,1}(t_2, t_3) = \mu_1 C_{1,1}(t_2, t_3), \quad (4.14)$$

where $\mu_1 = -\frac{a+i\omega_0}{b}$.

At order ε^2 . Equations (4.6) and (4.9) contain nonlinear terms. The absence of linear growth of the solution leads to $\partial_{t_1} C_{1,1} = \partial_{t_1} r_1 = 0$:

$$\begin{cases} \partial_{t_0} r_2 = -ar_2 - b(r_0\theta_2) + f_2(t_0, t_1, t_2, t_3) \\ \partial_{t_0} (r_0\theta_2) = -cr_2 + a(r_0\theta_2) + g_2(t_0, t_1, t_2, t_3) \end{cases} \quad (4.15)$$

with f_2 and g_2 being two functions defined by

$$\begin{cases} f_2(t_0, t_1, t_2, t_3) = \frac{a\delta r_0}{2} \cos(2\omega_0 t_0) + \frac{a}{2r_0} r_1^2 + \frac{a}{r_0} (r_0\theta_1)^2 - \frac{b}{r_0} r_1 (r_0\theta_1), \\ g_2(t_0, t_1, t_2, t_3) = \frac{c\delta r_0}{2} \cos(2\omega_0 t_0) + \frac{3c}{2r_0} r_1^2 + \frac{b}{r_0} (r_0\theta_1)^2. \end{cases} \quad (4.16)$$

This leads to the solution

$$\begin{cases} r_2 = C_{2,0}|C_{1,1}|^2 + C_{2,1}e^{i\omega_0 t_0} + \text{c.c.} + (C_{2,2,1} + C_{2,2,2}C_{1,1}^2)e^{2i\omega_0 t_0} + \text{c.c.}, \\ (r_0\theta_2) = D_{2,0}|C_{1,1}|^2 + D_{2,1}e^{i\omega_0 t_0} + \text{c.c.} + (D_{2,2,1} + D_{2,2,2}C_{1,1}^2)e^{2i\omega_0 t_0} + \text{c.c.}, \end{cases} \quad (4.17)$$

where $C_{2,0}$, $C_{2,2,1}$, $C_{2,2,2}$, $D_{2,0}$, $D_{2,2,1}$, $D_{2,2,2}$ are complex constants. Their values are computed and details are given in Appendix B.

At order ε^3 . Equations (4.7) and (4.10) lead to the following system of equations:

$$\begin{cases} \partial_{t_0} r_3 = -ar_3 - b(r_0\theta_3) + f_3(t_0, t_1, t_2, t_3), \\ \partial_{t_0} (r_0\theta_3) = -cr_3 + a(r_0\theta_3) + g_3(t_0, t_1, t_2, t_3), \end{cases} \quad (4.18)$$

where f_3 and g_3 are the functions

$$\begin{cases} f_3 = -\partial_{t_2} r_1 + \frac{ar_1 r_2}{r_0} - \frac{ar_1^3}{2r_0^2} - \frac{a\delta r_1 \cos(2\omega_0 t_0)}{2} - \frac{b(r_2(r_0\theta_1) + r_1(r_0\theta_2))}{r_0} + \frac{ar_1(r_0\theta_1)^2}{r_0^2} \\ \quad + \frac{2a(r_0\theta_1)(r_0\theta_2)}{r_0} + \frac{2b(r_0\theta_1)^3}{3r_0^2} - a\delta r_0 \omega_0 t_1 \sin(2\omega_0 t_0) \\ g_3 = -\partial_{t_2} (r_0\theta_1) + \frac{3cr_1 r_2}{r_0} - \frac{2cr_1^3}{r_0^2} - c\delta r_1 \cos(2\omega_0 t_0) - \frac{2a(r_0\theta_1)^3}{3r_0^2} + \frac{2b(r_0\theta_1)(r_0\theta_2)}{r_0} \\ \quad - c\delta \omega_0 t_1 \sin(2\omega_0 t_0). \end{cases} \quad (4.19)$$

This yields (see Appendix B) a differential equation on $C_{1,1}(t_2)$, called the amplitude equation. This equation governs the evolution of the amplitude of a perturbation from the vortex source around the neutral equilibrium point:

$$\partial_{t_2} C_{1,1} = (\underline{\mathbf{V}} + i\underline{\mathbf{VI}}) \overline{\delta C_{1,1}} + (\underline{\mathbf{VII}} + i\underline{\mathbf{VIII}}) |C_{1,1}|^2 C_{1,1}, \quad (4.20)$$

where $\underline{\mathbf{V}}$, $\underline{\mathbf{VI}}$, $\underline{\mathbf{VII}}$, $\underline{\mathbf{VIII}}$ are real constants computed in Appendix B. For $\Gamma_0 = -0.5$, $S_0 = \pm 0.01$, $\Omega = 1$ and $A = 0.8$ (two sets of parameters related to conditions (3.15), corresponding to the upper left case of Fig. 2, which we generically use in further numerical applications) we have $\underline{\mathbf{V}} \simeq \mp 3.00 \cdot 10^{-3}$, $\underline{\mathbf{VI}} \simeq 1.33 \cdot 10^{-1}$, $\underline{\mathbf{VII}} \simeq \pm 3.77 \cdot 10^{-2}$ and $\underline{\mathbf{VIII}} \simeq 3.35 \cdot 10^{-1}$.

4.1.2. Study of the amplitude equation

To study the slow-time variation of $C_{1,1}$, we set $C_{1,1} = ue^{i\beta}$ or $C_{1,1} = X + iY$ such that $\partial_{t_2} C_{1,1} = (\partial_{t_2} u + iu\partial_{t_2}\beta)e^{i\beta} = \partial_{t_2} X + i\partial_{t_2} Y$ (the polar form is of interest for determining the equilibria; the Cartesian form is simpler to analyze the stability of these equilibria). Using the polar form and separating the real and imaginary parts yields

$$\begin{cases} \partial_{t_2} u \cos \beta - u\partial_{t_2} \beta \sin \beta = u [(\delta\underline{\mathbf{V}} + u^2\underline{\mathbf{VIII}}) \cos \beta + (\delta\underline{\mathbf{VI}} + u^2\underline{\mathbf{VII}}) \sin \beta] \\ \partial_{t_2} u \sin \beta + u\partial_{t_2} \beta \cos \beta = u [(\delta\underline{\mathbf{VI}} + u^2\underline{\mathbf{VIII}}) \cos \beta + (-\delta\underline{\mathbf{V}} + u^2\underline{\mathbf{VII}}) \sin \beta] \end{cases} \quad (4.21)$$

equivalent to:

$$\begin{pmatrix} \partial_{t_2} u \\ u\partial_{t_2} \beta \end{pmatrix} = u\delta \begin{pmatrix} \cos(2\beta) & \sin(2\beta) \\ -\sin(2\beta) & \cos(2\beta) \end{pmatrix} \begin{pmatrix} \underline{\mathbf{V}} \\ \underline{\mathbf{VI}} \end{pmatrix} + u^3 \begin{pmatrix} \underline{\mathbf{VII}} \\ \underline{\mathbf{VIII}} \end{pmatrix}. \quad (4.22)$$

The equilibria $u_0 e^{i\beta_0}$ of this amplitude equation (see Fig. 3) are, from Eq. (4.22), either $u_0 = 0$ or they are given by

$$\delta \begin{pmatrix} \cos(2\beta_0) & \sin(2\beta_0) \\ -\sin(2\beta_0) & \cos(2\beta_0) \end{pmatrix} \begin{pmatrix} \underline{\mathbf{V}} \\ \underline{\mathbf{VI}} \end{pmatrix} + u_0^2 \begin{pmatrix} \underline{\mathbf{VII}} \\ \underline{\mathbf{VIII}} \end{pmatrix} = 0, \quad (4.23)$$

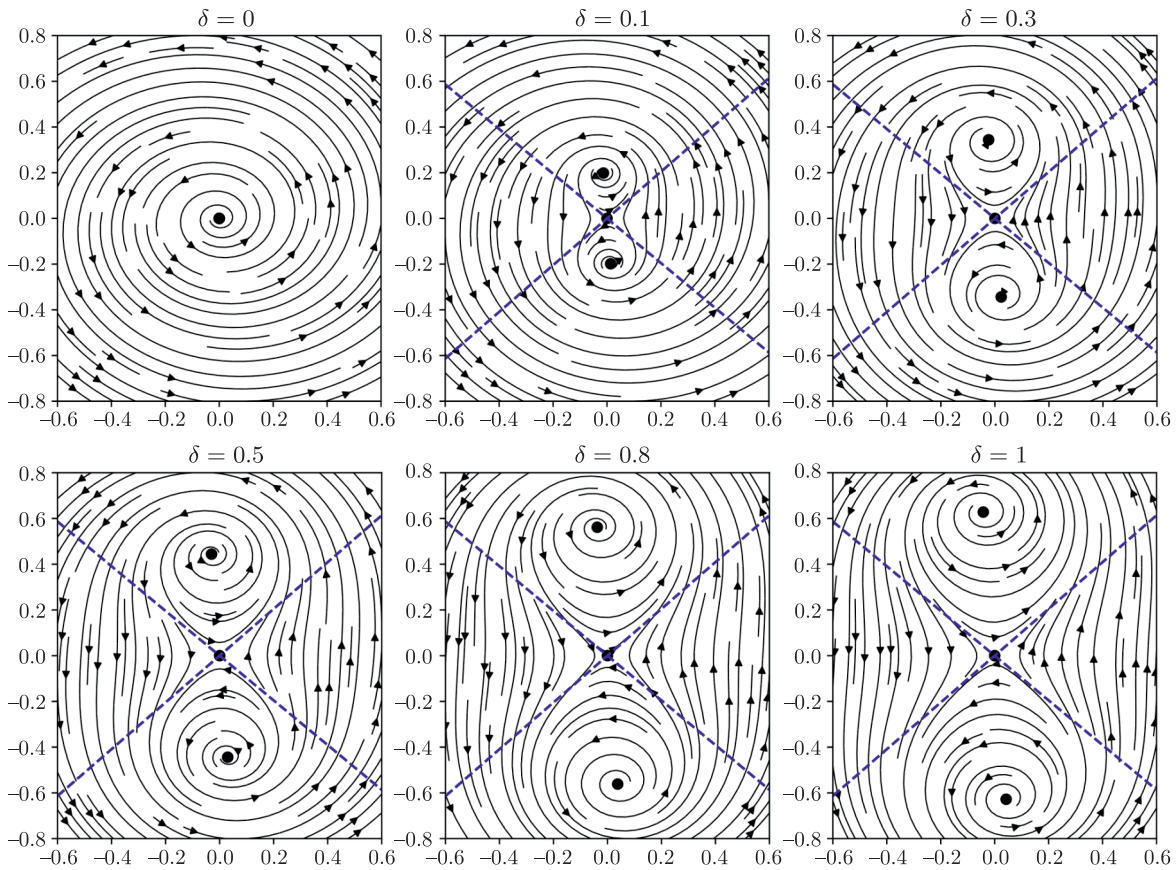


Fig. 3. Slow time evolution of $C_{1,1}(t_2) = X(t_2) + iY(t_2)$ for different values of δ . The blue dashed lines indicate the eigendirections of stability of the saddle equilibrium point $(0, 0)$. Here $S_0 = +0.01$, the other equilibrium points are repulsive.

leading to

$$\beta_0 = \frac{1}{2} \arctan \left[\frac{\text{VII VI} - \text{V VIII}}{\text{VIII VI} + \text{V VII}} \right] \pm \frac{\pi}{2} \simeq 3.86^\circ \pm 90^\circ, \tag{4.24}$$

$$u_0 = \sqrt{\delta} \left(\frac{\text{V}^2 + \text{VI}^2}{\text{VII}^2 + \text{VIII}^2} \right)^{\frac{1}{4}} \simeq 0.6293\sqrt{\delta}. \tag{4.25}$$

(where the numerical applications are done for our choice of physical parameters $\Gamma_0 = -0.5$, $S_0 = \pm 0.01$, $\Omega = 1$ and $A = 0.8$).

The stability analysis of these equilibria is easier calculated in Cartesian coordinates:

$$\begin{cases} \partial_{t_2} X = (\text{V}\delta + \text{VII}(X^2 + Y^2)) X + (\text{VI}\delta - \text{VIII}(X^2 + Y^2)) Y \\ \partial_{t_2} Y = (\text{VI}\delta + \text{VIII}(X^2 + Y^2)) X + (-\text{V}\delta + \text{VII}(X^2 + Y^2)) Y. \end{cases} \tag{4.26}$$

The Jacobian matrix of this system at the equilibrium point $(X_0, Y_0) = (u_0 \cos(\beta_0), u_0 \sin(\beta_0))$ is

$$M = \begin{pmatrix} \delta\text{V} + \text{VII}(3X_0^2 + Y_0^2) - 2X_0Y_0\text{VIII} & \delta\text{VI} - \text{VIII}(X_0^2 + 3Y_0^2) + 2X_0Y_0\text{VII} \\ \delta\text{VI} + \text{VIII}(3X_0^2 + Y_0^2) + 2X_0Y_0\text{VII} & -\delta\text{V} + \text{VII}(X_0^2 + 3Y_0^2) + 2X_0Y_0\text{VIII} \end{pmatrix}. \tag{4.27}$$

For the equilibrium point $(0, 0)$, the computation of the eigenvalues is straightforward: $\pm\delta\sqrt{\text{V}^2 + \text{VI}^2}$ and the eigendirections of this saddle point are represented in Fig. 3. As δ grows, two attractive or repulsive points appear and separate from each other in the plane. The nature of the centers depends

of the sign of S_0 . For this equilibrium, the numerical study of the real parts of the eigenvalues of the matrix M gives a linear and positive (resp. negative) value when $S_0 = +0.01$ (resp. $S_0 = -0.01$) with 0.02987 (resp. -0.02987) slope with respect to δ . This corresponds to the repulsive (resp. attractive) nature of the two equilibria.

4.2. Harmonic Forcing

In this subsection, the time variation of the circulation and source-sink magnitude is

$$\begin{cases} \Gamma(t_0, t_2) = \Gamma_0 (1 + \delta \varepsilon^3 \cos(\omega_0 t_0 + \omega_2 t_2)) \\ S(t_0, t_2) = S_0 (1 + \delta \varepsilon^3 \cos(\omega_0 t_0 + \omega_2 t_2)). \end{cases} \tag{4.28}$$

The multiple time scale expansion leads to the amplitude equation

$$\partial_{t_2} C_{1,1} = (\text{VII} + i\text{VIII}) |C_{1,1}|^2 C_{1,1} + \frac{(a - i\omega_0) r_0 \delta}{8} e^{i\omega_2 t_2}, \tag{4.29}$$

which is equivalent in polar coordinates ($C_{1,1} = u e^{i\beta}$) to

$$\begin{pmatrix} \partial_{t_2} u \\ u \partial_{t_2} \beta \end{pmatrix} = u^3 \begin{pmatrix} \text{VII} \\ \text{VIII} \end{pmatrix} - \frac{r_0 \delta}{8} \begin{pmatrix} -\cos(\beta - \omega_2 t_2) & \sin(\beta - \omega_2 t_2) \\ -\sin(\beta - \omega_2 t_2) & \cos(\beta - \omega_2 t_2) \end{pmatrix} \begin{pmatrix} a \\ \omega_0 \end{pmatrix}, \tag{4.30}$$

or in Cartesian coordinates ($C_{1,1} = X + iY$) to

$$\begin{pmatrix} \partial_{t_2} X \\ \partial_{t_2} Y \end{pmatrix} = (X^2 + Y^2) \begin{pmatrix} \text{VII} & -\text{VIII} \\ \text{VIII} & \text{VII} \end{pmatrix} \begin{pmatrix} X \\ Y \end{pmatrix} + \frac{r_0 \delta}{8} \begin{pmatrix} \cos(\omega_2 t_2) & \sin(\omega_2 t_2) \\ \sin(\omega_2 t_2) & -\cos(\omega_2 t_2) \end{pmatrix} \begin{pmatrix} a \\ \omega_0 \end{pmatrix}. \tag{4.31}$$

For $\omega_2 = 0$, finding the equilibrium point $(X_0, Y_0) = (u_0 \cos(\beta_0), u_0 \sin(\beta_0))$ is straightforward (see Figs. 4 and 5) and we have

$$X_0 = \frac{r_0 \delta (-a\text{VII} + \omega_0\text{VIII})}{8u_0^2 (\text{VII}^2 + \text{VIII}^2)}, \quad Y_0 = \frac{r_0 \delta (a\text{VIII} + \omega_0\text{VII})}{8u_0^2 (\text{VII}^2 + \text{VIII}^2)}, \tag{4.32}$$

where

$$u_0^3 = \frac{r_0 \delta}{8} \sqrt{\frac{a^2 + \omega_0^2}{\text{VII}^2 + \text{VIII}^2}}. \tag{4.33}$$

Numerical evaluation gives

$$u_0 \simeq 0.510\delta^{\frac{1}{3}}, \quad X_0 \simeq 0.506\delta^{\frac{1}{3}}, \quad Y_0 \simeq \pm 0.062\delta^{\frac{1}{3}}, \tag{4.34}$$

for $\Gamma_0 = -0.5$, $S_0 = \pm 0.01$, $\Omega = 1$ and $A = 0.8$.

Analyzing the stability of this equilibrium point, we find two complex conjugate eigenvalues of the following matrix:

$$M = \begin{pmatrix} \text{VII}(3X_0^2 + Y_0^2) - 2\text{VIII}X_0Y_0 & -\text{VIII}(X_0^2 + 3Y_0^2) + 2\text{VII}X_0Y_0 \\ \text{VIII}(3X_0^2 + Y_0^2) + 2\text{VII}X_0Y_0 & \text{VII}(X_0^2 + 3Y_0^2) + 2\text{VIII}X_0Y_0 \end{pmatrix}, \tag{4.35}$$

which are $(X_0^2 + Y_0^2) (2\text{VII} \pm i\sqrt{3\text{VIII}^2 - \text{VII}^2})$. Again, the real parts are positive or negative depending on the sign of S_0 . For the set of parameters we have chosen, it is a repulsive equilibrium point if $S_0 = +0.01$, and it is an attractive equilibrium point if $S_0 = -0.01$, as we can see in Figs. 4 and 5. Around those points, the oscillation pulsation is

$$\tilde{\omega}_2 = (X_0^2 + Y_0^2) \sqrt{3\text{VIII}^2 - \text{VII}^2} = (r_0 \delta)^{\frac{2}{3}} \left(\frac{a^2 + \omega_0^2}{\text{VII}^2 + \text{VIII}^2} \right)^{\frac{1}{3}} \frac{\sqrt{3\text{VIII}^2 - \text{VII}^2}}{4} \simeq 0.150 \delta^{\frac{2}{3}} \tag{4.36}$$

for the set of parameters we chose, independently of the sign of S_0 .

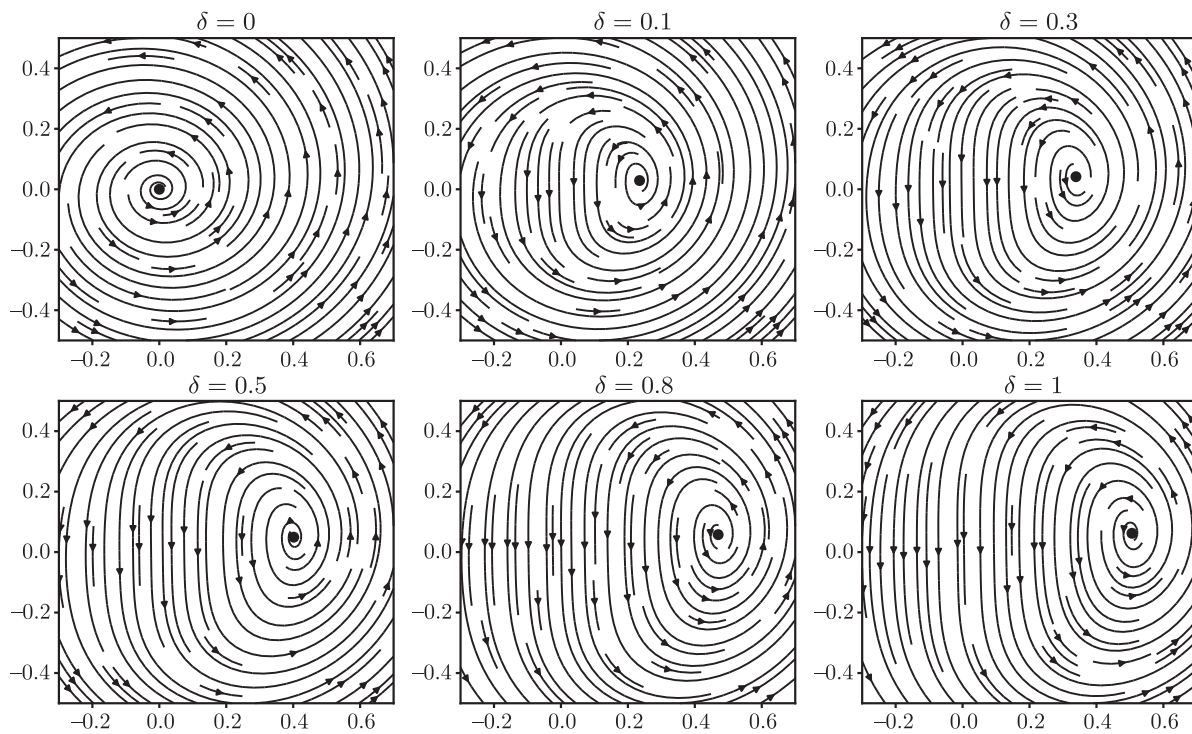


Fig. 4. Slow time evolution of $C_{1,1}(t_2) = X(t_2) + iY(t_2)$ for the harmonic forcing in the case $\omega_2 = 0$ and for $S_0 = +0.01$.

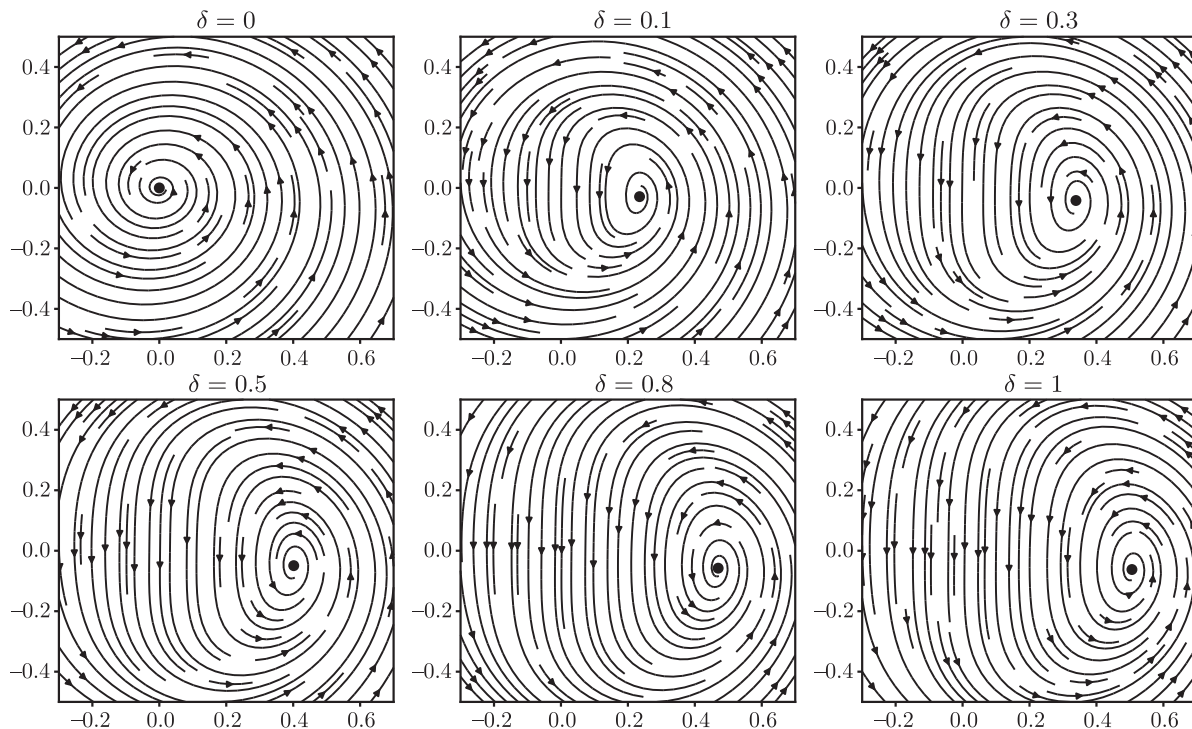


Fig. 5. Slow time evolution of $C_{1,1}(t_2) = X(t_2) + iY(t_2)$ for the harmonic forcing in the case $\omega_2 = 0$ and for $S_0 = -0.01$.

When $\omega_2 \neq 0$, the behavior of the system changes radically if we are in a source system ($S_0 > 0$) or a sink system ($S_0 < 0$), as we can see in the following figures (Figs. 6 and 7).

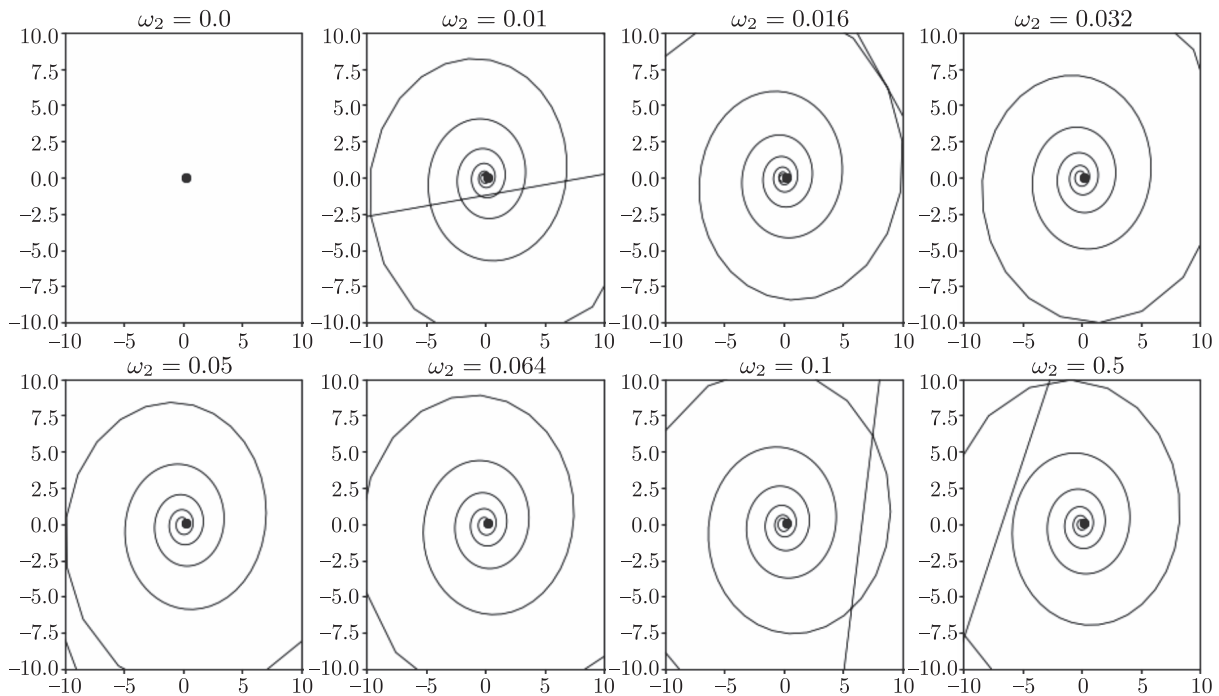


Fig. 6. Trajectories of $C_{1,1}$ for the harmonic forcing in the function of ω_2 for $\delta = 0.1$ (then $\tilde{\omega}_2 = 0.016$). The starting point is at the equilibrium point when $\omega_2 = 0$. The source is $S_0 = +0.01$. The straight lines indicate a numerical divergence of the trajectories. The equilibrium point is highly unstable. The calculation time is $T_f = 500$.

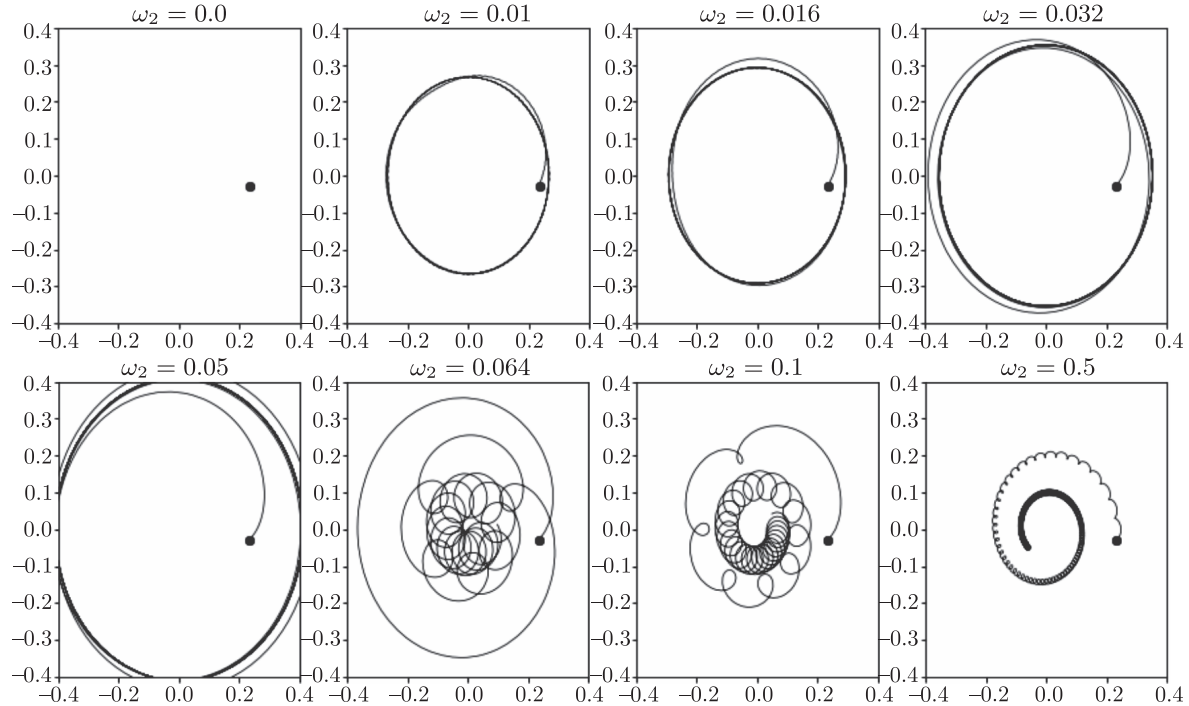


Fig. 7. Trajectories of $C_{1,1}$ for the harmonic forcing in the function of ω_2 for $\delta = 0.1$ (then $\tilde{\omega}_2 \sim 0.016$). The starting point is at the equilibrium point when $\omega_2 = 0$. The source is a sink $S_0 = -0.01$ and we can see a stabilization of $C_{1,1}$ with time. The equilibrium point is stable. The calculation time is $T_f = 2000$. For large ω_2 , it is likely from numerical simulations that $C_{1,1} \rightarrow 0$ as $t \rightarrow \infty$.

5. IMPACT OF THE SOURCE/CIRCULATION VARIABILITY ON THE TRAJECTORIES OF THE VORTEX SOURCES AND OF PASSIVE TRACERS

In this section, we compute numerically the evolution of the point vortex sources (or vortex sinks) and of passive tracers, advected by the total velocity field, when we vary ε . The results are quite similar for the subharmonic or the harmonic case, so we will only present the results for the subharmonic variability.

5.1. Point Vortex Trajectories

First, we study the trajectory of the point vortex sources before considering the evolution of the passive tracers. Figures 8 and 9 are built using a 4th-order Runge–Kutta scheme and show the evolution of one of the two point vortex sources (or vortex sinks) around the center of the stationary problem, as ε is increased. When $\varepsilon = 0$, we observe the rotation of the point vortex around the neutral equilibrium (the center). When increasing slightly ε , the vortex spirals outwards from its initial position. This is another illustration of the result previously shown (in Fig. 3): as ε is increased, the neutral point evolves into two repulsive centers. The slow time evolution is an increase in the modulus of C_{11} . Still, our analytical model holds only for weakly nonlinear evolutions and for small ε . The point vortex-source evolution for finite values of ε can only be described numerically. In particular, for $\varepsilon = 0.5$, vortex sinks leave the vicinity of the neutral point to drift towards the plane center. For large ε ($\varepsilon \geq 0.4$), the point vortex trajectories intersect and the dynamical system becomes irregular. Furthermore, these trajectories are noticeably different for a vortex source and for a vortex sink. In the latter case, the trajectory spirals around the plane center.

5.2. Passive Tracer Trajectories

After determining the vortex-source trajectories, we obtain those of passive tracers using also a 4th-order Runge–Kutta scheme. As a first indication for the possible trajectories of a passive tracer embedded in the time-varying flow, we compute the streamlines of the total flow, for vortex sources at the steady neutral points in Fig. 10. This figure helps position tracers initially. In particular, we see that the topology of the flow is comprised of 6 regions, five of them being compact and symmetric around the plane center, and the external trajectories circling these five regions. These regions enclose five centers and four hyperbolic (saddle) points.

Remark 5. The evolution of a passive tracer (in blue in Figs. 11 and 12) is not that of a vortex source. The tracer is advected by the two vortex sources simultaneously.

Using Fig. 10, we place passive tracers either near the plane center, or near a neutral point, or in the external region, far away from the plane center, see Figs. 11 and 12. In these figures, the evolution of point vortex source 1 is plotted in black; this vortex lies initially at the neutral point (which is no more an equilibrium point for $\varepsilon > 0$). For $\varepsilon = 0$, the tracer follows a closed curve around the plane center. For the point-vortex source, we can clearly see that the tracers' trajectories move out of the closed regions indicated in Fig. 10 when $\varepsilon = 0.5$. Such a finite amplitude variation of the source strength can be attained when induced by wind variability. It is clear that the tracers are mixed between the various regions. For an oceanographic application, this indicates that finite-area vortices would exchange their water masses in this case.

For a vortex sink, as mentioned previously, passive particles initially located around a neutral center can drift towards the center of the plane (for $\varepsilon = 0.4$); this indicates that mixing will be even more efficient in this case.

To measure the mixing of the tracers, we compute the trajectories of 100 passive particles initially close to each other and we calculate the time evolution of their RMS (root-mean square) relative distance. Figure 13 shows the motion and the growth in time of a patch of tracers. It indicates that the standard deviation grows initially exponentially fast, with a characteristic time $T = 25$. The subsequent growth (at $t = 75$) is even faster. A more detailed view of the growth of the patches is provided on Fig. 14. The initial position of the four patches of particles is indicated on Fig. 10. At long time, the growth of the tracer patch is similar for $\varepsilon = 0$ and for $\varepsilon = 0.2$, but at shorter time the patch shown on Fig. 13 grows exponentially fast for $\varepsilon = 0.2$.

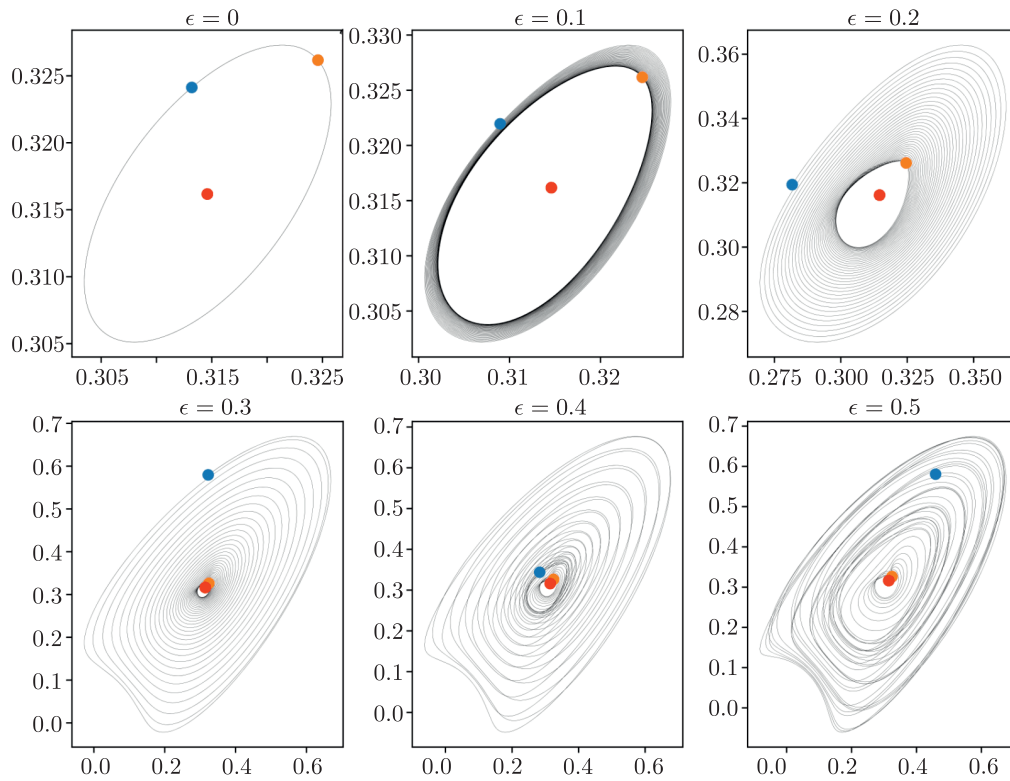


Fig. 8. Trajectories of the vortex source 1 for $\Gamma_0 = -0.5$, $S_0 = 0.01$, $\Omega = 1$ and $A = 0.8$. The red point is the center equilibrium point, the orange one is the initial position of the vortex and the blue one the position of the vortex at the calculation time $T_f = 300$.

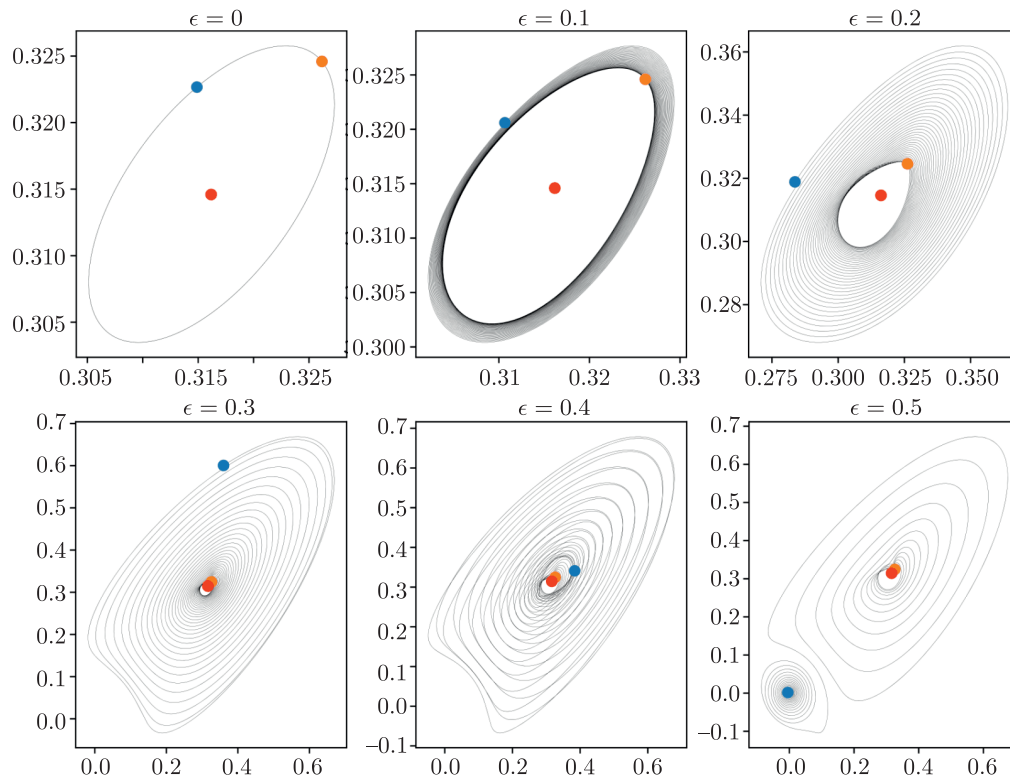


Fig. 9. Trajectories of the vortex sink 1 for $\Gamma_0 = -0.5$, $S_0 = -0.01$, $\Omega = 1$ and $A = 0.8$. The red point is the center equilibrium point, the orange one is the initial position of the vortex and the blue one the position of the vortex at the calculation time $T_f = 300$.

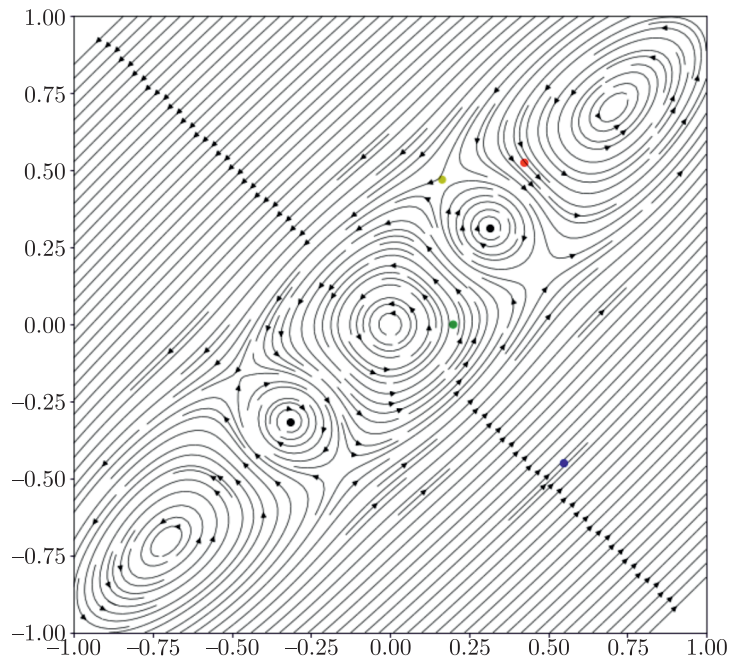


Fig. 10. Streamlines of the total flow when the two vortex sinks are placed at their equilibrium point (black points), for $\varepsilon = 0$ and for the usual parameters (here we take $S_0 = -0.01$ but it is really similar for the source case). We can see three center equilibrium points (one at the origin and two symmetric), four saddle points and two attractive equilibrium points (the center of the vortex sinks, they become repulsive equilibrium points if we take $S_0 > 0$). The four colored points are the starting points of the patch of tracers we used in the study.

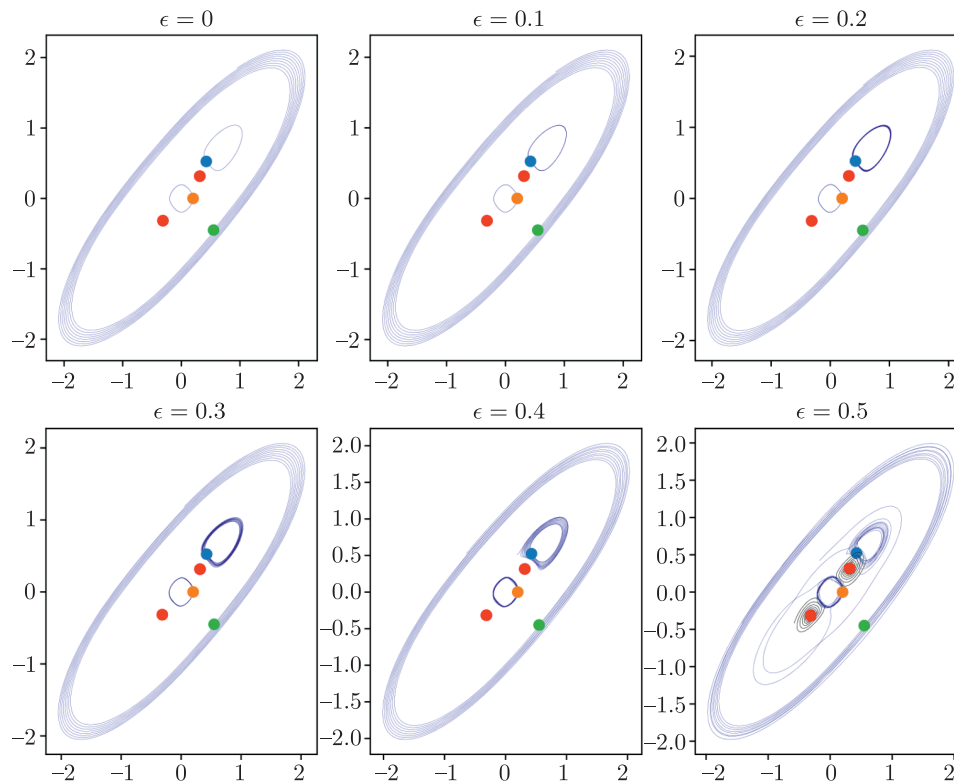


Fig. 11. Tracer evolution in the plane for a vortex-source system as ε is increased; in black: vortex-source trajectory; in blue: passive tracer trajectories. The red points are the initial position of the vortex sources at their center equilibrium points for $\varepsilon = 0$ and the blue, orange and green points are initial positions of the passive tracers. Here the calculation time is $T_f = 100$.

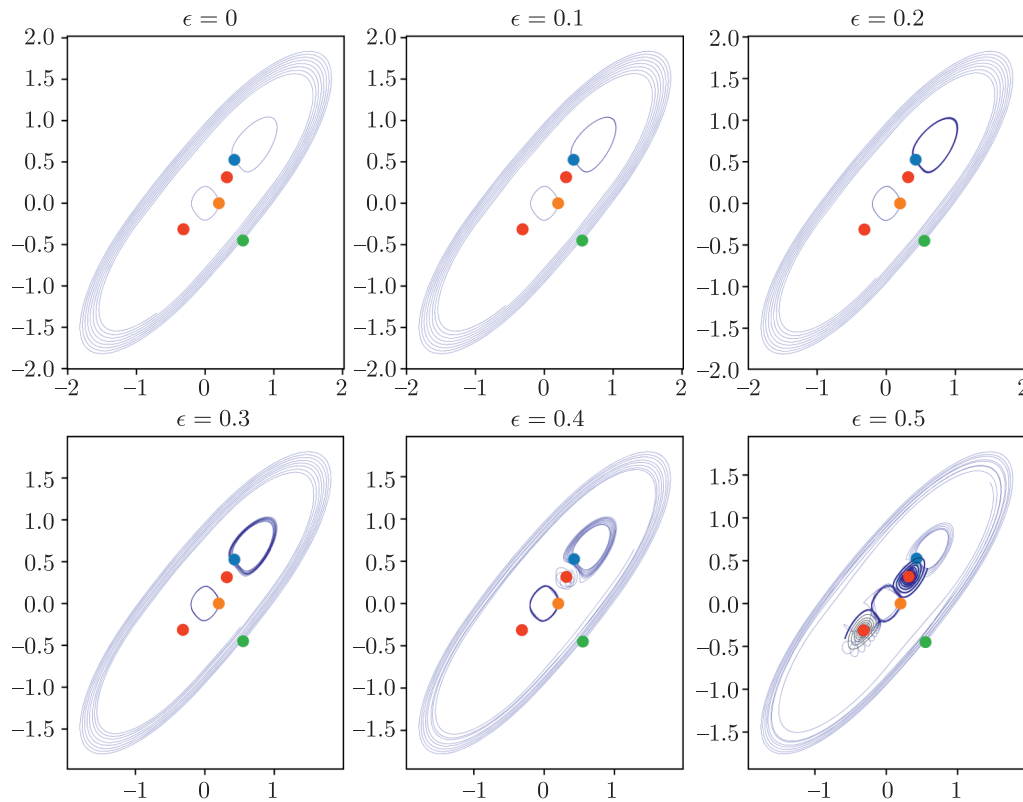


Fig. 12. Tracer evolution in the plane for a vortex-sink system as ε is increased. The colors are the same as in Fig. 11 and $T_f = 100$.

6. CONCLUSIONS, PERSPECTIVES AND PHYSICAL INTERPRETATIONS

In this paper, we have addressed the problem of two vortex sources in an external deformation field. Compared with previous studies, we have not considered a time-varying external flow but circulation and strength of the source/sink-vortices. We addressed the problem of point vortices analytically. This idealized situation, added to geometrical symmetry in the plane, allows the derivation and analysis of a simple dynamical system. For several values of the physical parameters, we have shown the existence of a center point of equilibrium around which the oscillation of the perturbed vortex occurs in a steady configuration.

We then have shown that a periodic variation of circulation or of the source flow, with a subharmonic or a harmonic frequency, could be caused by an unsteady wind. With such a variation of Γ or of S , we have calculated the slow evolution of the vortex trajectories from the steady orbit around the center point. The slow variation of the amplitude of the perturbation shows the destabilization of the center point into attractive or repulsive equilibria, for both the harmonic and subharmonic variations. The difference between these two cases is the number of equilibria (1 or 2). In both cases, the amplitude of the perturbation in the vicinity of these equilibria is bounded in time for small amplitudes of the time variation of Γ or of S . For larger amplitude variations (larger ε), trajectories are allowed between the previous fixed points. This indicates a transition to chaos when ε grows.

We have also computed the evolution and spreading of patches of passive particles. We have shown that the spreading can grow exponentially fast when the time variation of Γ or S is present. This indicates that the effect of an unsteady wind, taken into account via a relative wind stress, can increase the mixing of the fluid (here the oceanic fluid of the two vortices, or in their periphery). From this analysis alone, and considering previous studies, it is difficult to predict the exact influence of using the relative wind stress curl to force two interacting finite-area vortices. This will require numerical modeling with a detailed survey in the space of physical parameters as was done by Perrot and Carton [16]. In particular, the orientation of the background flow has been shown to have a crucial importance in facilitating or in reducing the vortex tendency to merge.

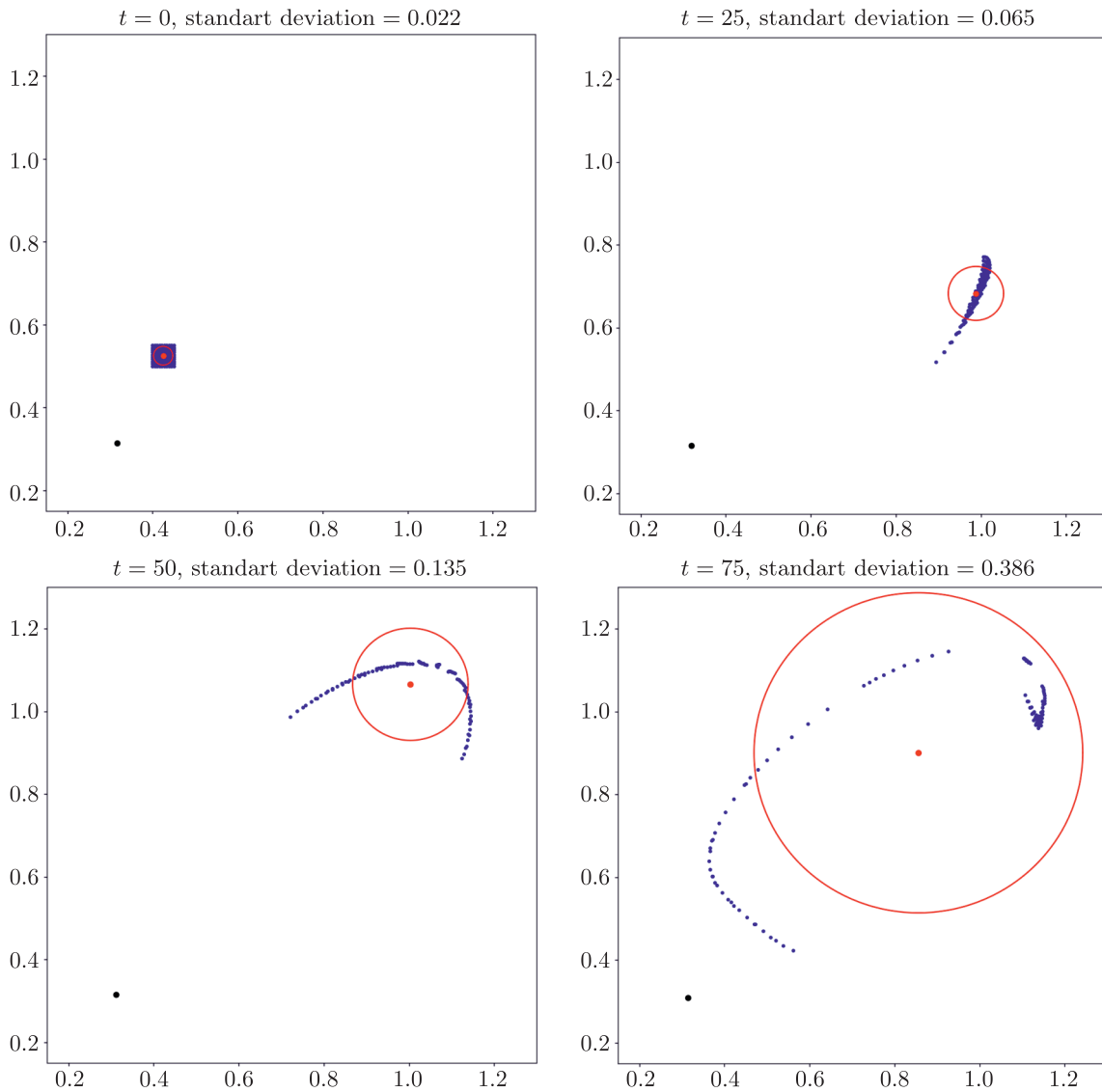


Fig. 13. Evolution of the vortex sink number 1 (black dot) close to its stable point. Evolution of 100 passive tracers (blue dots), of their global center (red dot) and of the standard deviation of the patch (represented by the red circle). For this experiment, $\varepsilon = 0.2$.

The orientation of the wind in our problem is related to the polarity of the source (source or sink) and it would be interesting to study its influence on vortex merger. This can be achieved using a fully coupled ocean-atmosphere quasi-geostrophic model, as a second step of this study. Another important aspect to be studied with a coupled model is the stability of individual, finite-area vortices. Indeed, both vortex interaction, which allows their growth (against the ambient shear of the surrounding flows which erode them), and the stability of isolated vortices are key mechanisms for the durability of these structures. Moreover, they make up the bulk of eddy kinetic energy in the ocean. Understanding eddy kinetic energy variations in coupled ocean-atmosphere models requires the knowledge of vortex processes in such models.

Ocean-atmosphere coupling creates an asymmetric Ekman pumping in the vortex and so the resultant of this pumping is not null and corresponds to a nondivergent free flow. The measure of this divergent component is impossible using altimetry because the speed computed from altimetry is geostrophic and so divergence-free. Surface buoys, ship drifts or other satellite sensors able to give complete speed are then needed. Future research will compare the total surface velocity field and the one deduced from altimetry and related to wind. This will allow us to better evaluate the impact on the divergence component of the flow on the vortex–vortex interactions.

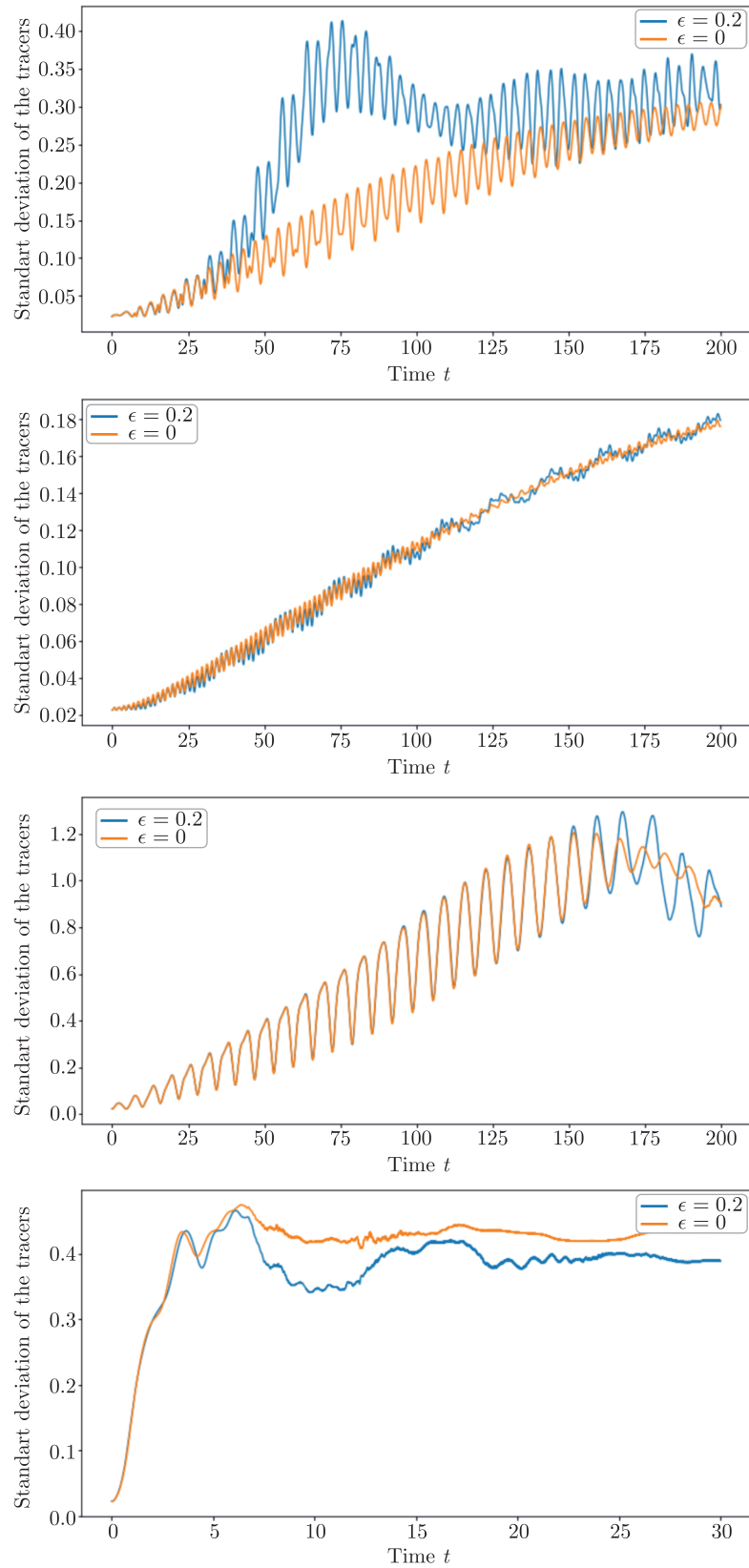


Fig. 14. Evolution of the standard deviation of the patch of tracers for different initial positions (those described in Fig. 10). The last one is for the initial position close to the saddle equilibrium point.

APPENDIX A. EQUILIBRIUM POINTS AND STABILITY

This section is a reminder of the fixed points of the problem; it was addressed slightly differently in [4] and in [3]. Recall the various cases for equilibria here with our notations and in our specific cases. This is necessary to further study the vortex source evolution with unsteady circulation or source strength.

Recall that we have the condition $\Gamma_0\Omega < 0$ and the formulas

$$\theta_0 = -\frac{1}{2} \arctan \left[\frac{\Gamma_0 + 4\pi r_0^2 \Omega}{S_0} \right], \quad (\text{A.1})$$

or

$$\theta_0 = -\frac{1}{2} \arctan \left[\frac{\Gamma_0 + 4\pi r_0^2 \Omega}{S_0} \right] + \frac{\pi}{2}, \quad (\text{A.2})$$

and

$$r_0^4(\Omega^2 - A^2) + \frac{\Gamma_0\Omega}{2\pi}r_0^2 + \frac{S_0^2 + \Gamma_0^2}{16\pi^2} = 0. \quad (\text{A.3})$$

6.1. For $\Omega^2 = A^2$:

Equilibrium. Starting from Eq. (A.3) with $\Omega^2 = A^2$ and $\Gamma_0\Omega < 0$, we have $r_0^2 = -\frac{S_0^2 + \Gamma_0^2}{8\pi\Gamma_0\Omega} > 0$ and thanks to Eq. (A.1), we have

$$r_0 = \sqrt{\frac{S_0^2 + \Gamma_0^2}{8\pi(-\Gamma_0\Omega)}} \quad \text{and} \quad \theta_0 = \frac{1}{2} \arctan \left[\frac{S_0^2 - \Gamma_0^2}{2S_0\Gamma_0} \right]. \quad (\text{A.4})$$

Stability. Is the equilibrium (A.4) stable? From the characteristic polynomial (3.7) of the differential matrix $\chi(X) = X^2 - \frac{S_0^2 + \Gamma_0^2 + 4\pi r_0^2 \Gamma_0 \Omega}{4\pi^2 r_0^4}$, we need to determine the sign of Δ_0 :

$$\Delta_0 = S_0^2 + \Gamma_0^2 + 4\pi r_0^2 \Gamma_0 \Omega = \frac{S_0^2 + \Gamma_0^2}{2} > 0. \quad (\text{A.5})$$

So χ has two real roots: one positive and one negative. Then the equilibrium (A.4) is a saddle equilibrium point. We are not interested in this type of equilibrium.

6.2. For $\Omega^2 \neq A^2$:

From the polynomial equation (A.3) in r_0^2 :

$$(\Omega^2 - A^2) X^2 + \frac{\Gamma_0\Omega}{2\pi} X + \frac{S_0^2 + \Gamma_0^2}{16\pi^2} = 0, \quad (\text{A.6})$$

we compute the discriminant

$$\Delta = \frac{1}{4\pi^2} [\Gamma_0^2 \Omega^2 - (S_0^2 + \Gamma_0^2) (\Omega^2 - A^2)], \quad (\text{A.7})$$

and look at the sign of

$$\Delta' = A^2 (S_0^2 + \Gamma_0^2) - S_0^2 \Omega^2, \quad (\text{A.8})$$

$$\Delta' = S_0^2 (A^2 - \Omega^2) + A^2 \Gamma_0^2. \quad (\text{A.9})$$

We want Δ' to be positive because we want real (positive) solutions to Eq. (A.6). This brings three situations (we have already studied the situation $\Omega^2 = A^2$):

- If $A^2 > \Omega^2$, then $\Delta' > 0$ clearly from Eq. (A.9).
- If $\Omega^2 > A^2$, then $\Delta' > 0 \iff \Omega^2 < A^2 \left(1 + \frac{\Gamma_0^2}{S_0^2}\right)$.
- If $\Omega^2 = A^2 \left(1 + \frac{\Gamma_0^2}{S_0^2}\right)$, then $\Delta' = 0$.

6.2.1. For $A^2 > \Omega^2$:

Because $A^2 > \Omega^2$, we have $\Delta' > 0$ without any more condition, and we have two solutions to the polynomial equation (A.6):

$$X_{\pm} = \frac{\Gamma_0\Omega \pm \sqrt{\Delta'}}{4\pi(A^2 - \Omega^2)}. \tag{A.10}$$

Recall that we want only a nonnegative solution ($r_0^2 > 0$). Because we have supposed the condition $\Gamma_0\Omega < 0$, this constraint removes X_- . The root X_+ is a nonnegative solution if and only if $\sqrt{\Delta'} > -\Gamma_0\Omega > 0$. This condition is valid because $(A^2 - \Omega^2)(S_0^2 + \Gamma_0^2) > 0$ so $\Delta' > \Gamma_0^2\Omega^2$.

Equilibrium for X_+ . We have the following equilibrium point (with θ_0 computed from Eq. (A.1)):

$$r_0 = \sqrt{\frac{\Gamma_0\Omega + \sqrt{\Delta'}}{4\pi(A^2 - \Omega^2)}} \quad \text{and} \quad \theta_0 = -\frac{1}{2} \arctan \left[\frac{\Gamma_0A^2 + \Omega\sqrt{\Delta'}}{S_0(A^2 - \Omega^2)} \right]. \tag{A.11}$$

Stability for X_+ . How is the equilibrium (A.11) stable? We need to know the sign of Δ_0 .

Proposition 1. *Under all the conditions of this subsection, we have*

$$\Delta_0 = S_0^2 + \Gamma_0^2 + 4\pi r_0^2 \Gamma_0\Omega > 0$$

and the equilibrium point (A.11) is a saddle equilibrium point.

Proof. Remember that we work under the assumption $A^2 > \Omega^2$ and $\Gamma_0\Omega < 0$. Then put r_0^2 in Δ_0 and

$$\begin{aligned} \Delta_0 > 0 &\iff (S_0^2 + \Gamma_0^2)(A^2 - \Omega^2) + \Gamma_0^2\Omega^2 > -\Gamma_0\Omega\sqrt{\Delta'} \\ &\iff [S_0^2(A^2 - \Omega^2) + \Gamma_0^2A^2]^2 > \Gamma_0^2\Omega^2S_0^2(A^2 - \Omega^2) + \Gamma_0^4\Omega^2A^2 \\ &\iff S_0^4(A^2 - \Omega^2) + S_0^2\Gamma_0^2(2A^2 - \Omega^2) + \Gamma_0^4A^2 > 0. \end{aligned}$$

The right-hand side of the equivalence is true under the assumption $A^2 > \Omega^2$. This concludes the proof of the proposition. \square

6.2.2. For $A^2 < \Omega^2 < A^2\left(1 + \frac{\Gamma_0^2}{S_0^2}\right)$:

We also have two roots of the polynomial (A.6):

$$X_{\pm} = \frac{-\Gamma_0\Omega \pm \sqrt{\Delta'}}{4\pi(\Omega^2 - A^2)}. \tag{A.12}$$

X_+ is clearly nonnegative. X_- is also nonnegative because we have $-\Gamma_0\Omega > \sqrt{\Delta'} > 0$ (deduced from the hypothesis). So we have two situations to analyze:

Equilibrium and stability for X_+ . We have the following equilibrium point (with θ_0 computed from Eq. (A.1)):

$$r_0 = \sqrt{\frac{-\Gamma_0\Omega + \sqrt{\Delta'}}{4\pi(\Omega^2 - A^2)}} \quad \text{and} \quad \theta_0 = \frac{1}{2} \arctan \left[\frac{\Gamma_0A^2 - \Omega\sqrt{\Delta'}}{S_0(\Omega^2 - A^2)} \right]. \tag{A.13}$$

How is this equilibrium (A.13) stable? We need to know the sign of Δ_0 .

Proposition 2. *Whatever the set of parameters we choose, if they satisfy the assumptions we made: $A^2 < \Omega^2 < A^2\left(1 + \frac{\Gamma_0^2}{S_0^2}\right)$ and $\Gamma_0\Omega < 0$, then we have*

$$\Delta_0 = S_0^2 + \Gamma_0^2 + 4\pi r_0^2 \Gamma_0\Omega < 0, \tag{A.14}$$

and the equilibrium point (A.13) is a neutral equilibrium point.

Proof. Consider Δ_0 for the value r_0 we have in Eq. (A.13):

$$\Delta_0 = S_0^2 + \Gamma_0^2 + \Gamma_0\Omega \left(\frac{-\Gamma_0\Omega + \sqrt{\Delta'}}{\Omega^2 - A^2} \right).$$

So

$$\begin{aligned} \Delta_0 < 0 &\iff (S_0^2 + \Gamma_0^2) (\Omega^2 - A^2) - \Gamma_0^2\Omega^2 + \Gamma_0\Omega\sqrt{\Delta'} < 0 \\ &\iff S_0^2 (\Omega^2 - A^2) + \Gamma_0^2A^2 + \Gamma_0\Omega\sqrt{\Delta'} < 0. \end{aligned}$$

The right-hand side of the equivalence is true because $\Gamma_0\Omega < 0$ and $\Omega^2 - A^2 < A^2 \frac{\Gamma_0^2}{S_0^2}$ so $S_0^2 (\Omega^2 - A^2) + \Gamma_0^2A^2 < 0$. This concludes the proof of the proposition. \square

Equilibrium and stability for X_- . We have the following equilibrium point (with θ_0 computed from Eq. (A.1)):

$$r_0 = \sqrt{\frac{-\Gamma_0\Omega - \sqrt{\Delta'}}{4\pi(\Omega^2 - A^2)}} \quad \text{and} \quad \theta_0 = \frac{1}{2} \arctan \left[\frac{\Gamma_0A^2 + \Omega\sqrt{\Delta'}}{S_0(\Omega^2 - A^2)} \right]. \tag{A.15}$$

Proposition 3. *For the equilibrium (A.15), Δ_0 is nonnegative for every set of parameters such that $A^2 < \Omega^2 < A^2 \left(1 + \frac{\Gamma_0^2}{S_0^2}\right)$ and $\Gamma_0\Omega < 0$. So the equilibrium (A.15) is a saddle equilibrium point.*

Proof. Look at the expression of Δ_0 :

$$\Delta_0 = S_0^2 + \Gamma_0^2 + 4\pi r_0^2 \Gamma_0\Omega = S_0^2 + \Gamma_0^2 + \frac{-\Gamma_0^2\Omega^2 - \Gamma_0\Omega\sqrt{\Delta'}}{\Omega^2 - A^2}, \tag{A.16}$$

in which the sign is the same as the sign of

$$(S_0^2 + \Gamma_0^2) (\Omega^2 - A^2) - \Gamma_0^2\Omega^2 - \Gamma_0\Omega\sqrt{\Delta'} = \underbrace{S_0^2 (\Omega^2 - A^2) - \Gamma_0^2A^2}_{<0 \text{ because } \Omega^2 - A^2 < A^2 \frac{\Gamma_0^2}{S_0^2}} + \underbrace{(-\Gamma_0\Omega\sqrt{\Delta'})}_{>0}. \tag{A.17}$$

So we have the following equivalences:

$$\begin{aligned} \Delta_0 > 0 &\iff -\Gamma_0\Omega\sqrt{\Delta'} > \Gamma_0^2A^2 - S_0^2 (\Omega^2 - A^2) \\ &\iff \Gamma_0^2\Omega^2\Delta' > (\Gamma_0^2A^2 - S_0^2 (\Omega^2 - A^2))^2 \\ &\iff \Gamma_0^2\Omega^2S_0^2 (A^2 - \Omega^2) + \Gamma_0^4A^2 (\Omega^2 - A^2) > -2\Gamma_0^2A^2S_0^2 (\Omega^2 - A^2) + S_0^4 (\Omega^2 - A^2)^2 \\ &\iff S_0^4 (\Omega^2 - A^2) + S_0^2\Gamma_0^2 (\Omega^2 - 2A^2) - \Gamma_0^4A^2 < 0. \end{aligned}$$

We have to study the sign of a second-degree polynomial in S_0^2 for which the discriminant is

$$\delta = \Gamma_0^4 (\Omega^2 - 2A^2)^2 + 4\Gamma_0^4A^2 (\Omega^2 - A^2) = \Gamma_0^4\Omega^4 > 0. \tag{A.18}$$

The two roots are

$$\frac{-\Gamma_0^2 (\Omega^2 - 2A^2) + \Gamma_0^2\Omega^2}{2(\Omega^2 - A^2)} = \frac{A^2\Gamma_0^2}{\Omega^2 - A^2} > 0, \tag{A.19}$$

and

$$\frac{-\Gamma_0^2 (\Omega^2 - 2A^2) - \Gamma_0^2\Omega^2}{2(\Omega^2 - A^2)} = -\Gamma_0^2 < 0. \tag{A.20}$$

Because $S_0^2 > 0$, to have $\Delta_0 > 0$, we need S_0^2 to be smaller than the largest root, but this is not an additional constraint because

$$S_0^2 < \frac{A^2\Gamma_0^2}{\Omega^2 - A^2} \iff (\Omega^2 - A^2) S_0^2 < A^2\Gamma_0^2$$

$$\iff \Omega^2 < A^2 \left(1 + \frac{\Gamma_0^2}{S_0^2} \right).$$

So the polynomial $(\Omega^2 - A^2) X^2 + \Gamma_0^2 (\Omega^2 - 2A^2) X - \Gamma_0^4 A^2$ is nonpositive for every value between 0 and $\frac{A^2 \Gamma_0^2}{\Omega^2 - A^2}$. Because S_0^2 is in this interval, we have $\Delta_0 > 0$ for every set of parameters such that $A^2 < \Omega^2 < A^2 \left(1 + \frac{\Gamma_0^2}{S_0^2} \right)$ and $\Gamma_0 \Omega < 0$. □

6.2.3. For $\Omega^2 = A^2 \left(1 + \frac{\Gamma_0^2}{S_0^2} \right)$

In this section, we have $\Delta' = 0$. Then there is only one solution to Eq. (A.6):

$$X = \frac{-\Gamma_0 \Omega}{4\pi(\Omega^2 - A^2)} = \frac{\Gamma_0^2 + S_0^2}{4\pi(-\Gamma_0 \Omega)} > 0. \tag{A.21}$$

This gives the following equilibrium point:

$$r_0 = \sqrt{\frac{\Gamma_0^2 + S_0^2}{4\pi(-\Gamma_0 \Omega)}} \quad \text{and} \quad \theta_0 = \frac{1}{2} \arctan \left(\frac{S_0}{\Gamma_0} \right). \tag{A.22}$$

To know the type of stability, we compute Δ_0 :

$$\Delta_0 = S_0^2 + \Gamma_0^2 + 4\pi r_0^2 \Gamma_0 \Omega = S_0^2 + \Gamma_0^2 + \Gamma_0 \Omega \frac{\Gamma_0^2 + S_0^2}{(-\Gamma_0 \Omega)} = 0. \tag{A.23}$$

So we cannot conclude about the stability of the equilibrium (A.22).

APPENDIX B. MULTIPLE TIME SCALE DEVELOPMENT

The multiple time scale method is here expanded for the subharmonic case. The harmonic case is similar.

6.1. Order ε^1

We have the following system at order ε^1 , computed from Eqs. (4.5) and (4.8):

$$\begin{cases} \partial_{t_0} r_1 = -ar_1 - b(r_0 \theta_1) \\ \partial_{t_0} (r_0 \theta_1) = -cr_1 + a(r_0 \theta_1). \end{cases} \tag{B.1}$$

So

$$\begin{cases} r_1 = C_{1,1}(t_2, t_3) e^{i\omega_0 t_0} + \text{c.c} \\ r_0 \theta_1 = D_{1,1}(t_2, t_3) e^{i\omega_0 t_0} + \text{c.c} \end{cases} \tag{B.2}$$

with

$$D_{1,1}(t_2, t_3) = \mu_1 C_{1,1}(t_2, t_3), \tag{B.3}$$

and $\mu_1 = -\frac{a+i\omega_0}{b}$.

6.2. Order ε^2

With Eqs. (4.6) and (4.9) and because $\partial_{t_1} r_1 = \partial_{t_1} (r_0 \theta_1) = 0$, we have the following system in $(r_2, r_0 \theta_2)$:

$$\begin{cases} \partial_{t_0} r_2 = -ar_2 - b(r_0 \theta_2) + f_2(t_0, t_1, t_2, t_3) \\ \partial_{t_0} (r_0 \theta_2) = -cr_2 + a(r_0 \theta_2) + g_2(t_0, t_1, t_2, t_3), \end{cases} \quad (\text{B.4})$$

where

$$\begin{cases} f_2(t_0, t_1, t_2, t_3) = \frac{a\delta r_0}{2} \cos(2\omega_0 t_0) + \frac{a}{2r_0} r_1^2 + \frac{a}{r_0} (r_0 \theta_1)^2 - \frac{b}{r_0} r_1 (r_0 \theta_1) \\ g_2(t_0, t_1, t_2, t_3) = \frac{c\delta r_0}{2} \cos(2\omega_0 t_0) + \frac{3c}{2r_0} r_1^2 + \frac{b}{r_0} (r_0 \theta_1)^2. \end{cases} \quad (\text{B.5})$$

The system (B.4) gives:

- For r_2 :

$$\begin{aligned} \partial_{t_0}^2 r_2 &= -a(-ar_2 - b(r_0 \theta_2) + f_2) - b(-cr_2 + a(r_0 \theta_2) + g_2) + \partial_{t_0} f_2 \\ &= (a^2 + bc) r_2 + h_2(t_0, t_1, t_2, t_3). \end{aligned} \quad (\text{B.6})$$

- For $r_0 \theta_2$:

$$\begin{aligned} \partial_{t_0}^2 (r_0 \theta_2) &= -c(-ar_2 - b(r_0 \theta_2) + f_2) + a(-cr_2 + a(r_0 \theta_2) + g_2) + \partial_{t_0} g_2 \\ &= (bc + a^2) (r_0 \theta_2) + k_2(t_0, t_1, t_2, t_3), \end{aligned} \quad (\text{B.7})$$

where

$$\begin{cases} h_2(t_0, t_1, t_2, t_3) = (-af_2 - bg_2 + \partial_{t_0} f_2)(t_0, t_1, t_2, t_3) \\ k_2(t_0, t_1, t_2, t_3) = (-cf_2 + ag_2 + \partial_{t_0} g_2)(t_0, t_1, t_2, t_3). \end{cases} \quad (\text{B.8})$$

- Development of f_2 :

$$\begin{aligned} f_2 &= \frac{a}{r_0} \left[3 - \frac{2c}{b} \right] |C_{1,1}|^2 \\ &\quad + \left[\frac{ar_0}{4} + \frac{C_{1,1}^2}{r_0} \left(\frac{3a}{2} + \frac{a(a+i\omega_0)^2}{b^2} + i\omega_0 \right) \right] e^{2i\omega_0 t_0} + \text{c.c.} \\ f_2 &= F_{2,0} |C_{1,1}|^2 + [F_{2,2,1} + F_{2,2,2} C_{1,1}^2] e^{2i\omega_0 t_0} + \text{c.c.} \end{aligned} \quad (\text{B.9})$$

- Development of g_2 :

$$\begin{aligned} g_2 &= \frac{c}{r_0} |C_{1,1}|^2 + \left[\frac{cr_0}{4} + \frac{C_{1,1}^2}{r_0} \left(\frac{3c}{2} + \frac{(a+i\omega_0)^2}{b} \right) \right] e^{2i\omega_0 t_0} + \text{c.c.} \\ g_2 &= G_{2,0} |C_{1,1}|^2 + [G_{2,2,1} + G_{2,2,2} C_{1,1}^2] e^{2i\omega_0 t_0} + \text{c.c.} \end{aligned} \quad (\text{B.10})$$

- Development of h_2 :

$$\begin{aligned} h_2 &= [-aF_{2,0} - bG_{2,0}] |C_{1,1}|^2 + [(-bG_{2,2,1} + (-a + 2i\omega_0) F_{2,2,1}) \\ &\quad + (-bG_{2,2,2} + (-a + 2i\omega_0) F_{2,2,2}) C_{1,1}^2] e^{2i\omega_0 t_0} + \text{c.c.} \\ h_2 &= H_{2,0} |C_{1,1}|^2 + [H_{2,2,1} + H_{2,2,2} C_{1,1}^2] e^{2i\omega_0 t_0} + \text{c.c.} \end{aligned} \quad (\text{B.11})$$

- Development of k_2 :

$$\begin{aligned}
 k_2 &= [-cF_{2,0} + aG_{2,0}] |C_{1,1}|^2 + [(-cF_{2,2,1} + (a + 2i\omega_0) G_{2,2,1}) \\
 &\quad + (-cF_{2,2,2} + (a + 2i\omega_0) G_{2,2,2}) C_{1,1}^2] e^{2i\omega_0 t_0} + \text{c.c} \\
 k_2 &= K_{2,0} |C_{1,1}|^2 + [K_{2,2,1} + K_{2,2,2} C_{1,1}^2] e^{2i\omega_0 t_0} + \text{c.c.}
 \end{aligned}
 \tag{B.12}$$

Then from Eqs. (B.6) and (B.7) we have

- The homogeneous solutions:

$$\begin{cases}
 r_2 = C_{2,1} e^{i\omega_0 t_0} + \text{c.c} \\
 (r_0 \theta_2) = D_{2,1} e^{i\omega_0 t_0} + \text{c.c}
 \end{cases}
 \tag{B.13}$$

- The particular solutions for the constant terms:

$$\begin{cases}
 r_2 = \frac{H_{2,0}}{\omega_0^2} |C_{1,1}|^2 \\
 (r_0 \theta_2) = \frac{K_{2,0}}{\omega_0^2} |C_{1,1}|^2
 \end{cases}
 \tag{B.14}$$

- The particular solutions for $e^{2i\omega_0 t_0} + \text{c.c.}$:

$$\begin{cases}
 r_2 = -\frac{H_{2,2,1} + H_{2,2,2} C_{1,1}^2}{3\omega_0^2} e^{2i\omega_0 t_0} + \text{c.c} \\
 (r_0 \theta_2) = -\frac{K_{2,2,1} + K_{2,2,2} C_{1,1}^2}{3\omega_0^2} e^{2i\omega_0 t_0} + \text{c.c.}
 \end{cases}
 \tag{B.15}$$

So the total solution of Eqs. (B.6) and (B.7) is

$$\begin{cases}
 r_2 = C_{2,0} |C_{1,1}|^2 + C_{2,1} e^{i\omega_0 t_0} + \text{c.c} + (C_{2,2,1} + C_{2,2,2} C_{1,1}^2) e^{2i\omega_0 t_0} + \text{c.c} \\
 (r_0 \theta_2) = D_{2,0} |C_{1,1}|^2 + D_{2,1} e^{i\omega_0 t_0} + \text{c.c} + (D_{2,2,1} + D_{2,2,2} C_{1,1}^2) e^{2i\omega_0 t_0} + \text{c.c}
 \end{cases}
 \tag{B.16}$$

with (for $i = 1, 2$)

$$C_{2,0} = \frac{H_{2,0}}{\omega_0^2}, \quad C_{2,2,i} = -\frac{H_{2,2,i}}{3\omega_0^2}, \quad D_{2,0} = \frac{K_{2,0}}{\omega_0^2}, \quad D_{2,2,i} = -\frac{K_{2,2,i}}{3\omega_0^2}.
 \tag{B.17}$$

6.3. Order ϵ^3

With Eqs. (4.7) and (4.10), we have the following system at the order ϵ^3 :

$$\begin{cases}
 \partial_{t_0} r_3 = -ar_3 - b(r_0 \theta_3) + f_3(t_0, t_1, t_2, t_3) \\
 \partial_{t_0} (r_0 \theta_3) = -cr_3 + a(r_0 \theta_3) + g_3(t_0, t_1, t_2, t_3),
 \end{cases}
 \tag{B.18}$$

where f_3 and g_3 are the following given functions:

$$\begin{cases}
 f_3 = -\partial_{t_2} r_1 + \frac{ar_1 r_2}{r_0} - \frac{ar_1^3}{2r_0^2} - \frac{ar_1 \cos(2\omega_0 t_0)}{2} - \frac{b(r_2(r_0 \theta_1) + r_1(r_0 \theta_2))}{r_0} + \frac{ar_1(r_0 \theta_1)^2}{r_0^2} \\
 \quad + \frac{2a(r_0 \theta_1)(r_0 \theta_2)}{r_0} + \frac{2b(r_0 \theta_1)^3}{3r_0^2} - ar_0 \omega_0 t_1 \sin(2\omega_0 t_0) \\
 g_3 = -\partial_{t_2} (r_0 \theta_1) + \frac{3cr_1 r_2}{r_0} - \frac{2cr_1^3}{r_0^2} - cr_1 \cos(2\omega_0 t_0) - \frac{2a(r_0 \theta_1)^3}{3r_0^2} + \frac{2b(r_0 \theta_1)(r_0 \theta_2)}{r_0} \\
 \quad - c\omega_0 t_1 \sin(2\omega_0 t_0).
 \end{cases}
 \tag{B.19}$$

The system (B.18) gives:

- For r_3 :

$$\begin{aligned} \partial_{t_0}^2 r_3 &= -a(-ar_3 - b(r_0\theta_3) + f_3) - b(-cr_3 + a(r_0\theta_3) + g_3) + \partial_{t_0} f_3 \\ &= (a^2 + bc)r_3 + h_3. \end{aligned} \tag{B.20}$$

- For $r_0\theta_3$:

$$\begin{aligned} \partial_{t_0}^2 (r_0\theta_3) &= -c(-ar_3 - b(r_0\theta_3) + f_3) + a(-cr_3 + a(r_0\theta_3) + g_3) + \partial_{t_0} g_3 \\ &= (bc + a^2)(r_0\theta_3) + k_3. \end{aligned} \tag{B.21}$$

We do not develop f_3 , g_3 , h_3 and k_3 as we did for the order ε^2 . We only introduce the following notations:

$$\begin{cases} f_3 = F_{3,0} + F_{3,1}e^{i\omega_0 t_0} + F_{3,2}e^{2i\omega_0 t_0} + F_{3,3}e^{3i\omega_0 t_0} + \text{c.c} \\ g_3 = G_{3,0} + G_{3,1}e^{i\omega_0 t_0} + G_{3,2}e^{2i\omega_0 t_0} + G_{3,3}e^{3i\omega_0 t_0} + \text{c.c} \\ h_3 = H_{3,0} + H_{3,1}e^{i\omega_0 t_0} + H_{3,2}e^{2i\omega_0 t_0} + H_{3,3}e^{3i\omega_0 t_0} + \text{c.c} \\ k_3 = K_{3,0} + K_{3,1}e^{i\omega_0 t_0} + K_{3,2}e^{2i\omega_0 t_0} + K_{3,3}e^{3i\omega_0 t_0} + \text{c.c}. \end{cases} \tag{B.22}$$

Then, if we denote by L the self-adjoint linear operator $\partial_{t_0}^2 + \omega_0^2$, we have $r_1^* L r_3 = r_1^* h_3 = r_1^* L^* r_3 = 0 = \langle r_1, h_3 \rangle$. But $\langle e^{in\omega_0 t_0}, e^{ip\omega_0 t_0} \rangle = \delta_{n,p}$ (Kronecker symbol) for $n, p \in \mathbf{Z}$ and because $r_1 = C_{1,1}e^{i\omega_0 t_0} + \text{c.c}$, we have

$$\langle r_1, h_3 \rangle = C_{1,1}H_{3,1} + \text{c.c} = 0. \tag{B.23}$$

Because $H_{3,1} = (-a + i\omega_0)F_{3,1} - bG_{3,1}$, we deduce the amplitude equation

$$(-a + i\omega_0)F_{3,1} - bG_{3,1} = 0. \tag{B.24}$$

So we only have to compute $F_{3,1}$ and $G_{3,1}$ from Eq. (B.19): writing

$$\begin{cases} F_{3,1} = -\partial_{t_2} C_{1,1} + \mathbf{I}\overline{C_{1,1}} + \mathbf{II}|C_{1,1}|^2 C_{1,1} \\ G_{3,1} = \frac{a+i\omega_0}{b}\partial_{t_2} C_{1,1} + \mathbf{III}\overline{C_{1,1}} + \mathbf{IV}|C_{1,1}|^2 C_{1,1}, \end{cases} \tag{B.25}$$

we have:

$$\mathbf{I} = -\frac{a}{4} + \frac{C_{2,2,1}}{r_0}(2a - i\omega_0) + \frac{D_{2,2,1}}{r_0}\left(-b - \frac{2a^2}{b} + \frac{2ai\omega_0}{b}\right), \tag{B.26}$$

$$\begin{aligned} \mathbf{II} &= \frac{1}{r_0^2} \left[a\left(-\frac{3}{2} + 2\frac{a^2}{b^2} + \frac{c}{b}\right) + 2i\omega_0\left(\frac{a^2}{b^2} + \frac{c}{b}\right) \right] \\ &\quad + \frac{C_{2,0}}{r_0}(2a + i\omega_0) + \frac{D_{2,0}}{r_0}\left(-b - \frac{2a^2}{b} - \frac{2ai\omega_0}{b}\right) \\ &\quad + \frac{C_{2,2,2}}{r_0}(2a - i\omega_0) + \frac{D_{2,2,2}}{r_0}\left(-b - \frac{2a^2}{b} + \frac{2ai\omega_0}{b}\right), \end{aligned} \tag{B.27}$$

$$\mathbf{III} = -\frac{c}{2} + \frac{3c}{r_0}C_{2,2,1} + \frac{2D_{2,2,1}}{r_0}(-a + i\omega_0), \tag{B.28}$$

$$\begin{aligned} \mathbf{IV} &= -\frac{6c}{r_0^2} - \frac{2ac}{r_0^2 b^2}(a + i\omega_0) + \frac{3c}{r_0}(C_{2,0} + C_{2,2,2}) \\ &\quad - \frac{2}{r_0}((a + i\omega_0)D_{2,0} + (a - i\omega_0)D_{2,2,2}). \end{aligned} \tag{B.29}$$

From Eq. (B.24) we obtain the amplitude equation

$$\partial_{t_2} C_{1,1} = (\mathbf{V} + i\mathbf{VI})\overline{C_{1,1}} + (\mathbf{VII} + i\mathbf{VIII})|C_{1,1}|^2 C_{1,1}, \tag{B.30}$$

with

$$\begin{cases} \mathbf{V} = \operatorname{Re} \left(-\frac{(a - i\omega_0)\mathbf{I} + b\mathbf{III}}{2i\omega_0} \right) \\ \mathbf{VI} = \operatorname{Im} \left(-\frac{(a - i\omega_0)\mathbf{I} + b\mathbf{III}}{2i\omega_0} \right) \\ \mathbf{VII} = \operatorname{Re} \left(-\frac{(a - i\omega_0)\mathbf{II} + b\mathbf{IV}}{2i\omega_0} \right) \\ \mathbf{VIII} = \operatorname{Im} \left(-\frac{(a - i\omega_0)\mathbf{II} + b\mathbf{IV}}{2i\omega_0} \right). \end{cases} \quad (\text{B.31})$$

ACKNOWLEDGMENTS

The first author thanks Ecole Normale Supérieure de Rennes (Maths Department) for a Ph.D. grant allowing the completion of this work.

The authors thank Dr Jean N. Reinaud for proofreading and the English writing of this paper.

CONFLICT OF INTEREST

The authors declare that they have no conflicts of interest.

REFERENCES

1. Aref, H., Integrable, Chaotic, and Turbulent Vortex Motion in Two-Dimensional Flows, *Annu. Rev. Fluid Mech.*, 1983, vol. 15, pp. 345–389.
2. Aref, H. and Pomphrey, N., Integrable and Chaotic Motions of Four Vortices, *Phys. Lett. A*, 1980, vol. 78, no. 4, pp. 297–300.
3. Bizyaev, I. A., Borisov, A. V., and Mamaev, I. S., The Dynamics of Vortex Sources in a Deformation Flow, *Regul. Chaotic Dyn.*, 2016, vol. 21, no. 3, pp. 367–376.
4. Borisov, A. V. and Mamaev, I. S., On the Problem of Motion Vortex Sources on a Plane, *Regul. Chaotic Dyn.*, 2006, vol. 11, no. 4, pp. 455–466.
5. Carton, X. J., Hydrodynamical Modelling of Oceanic Vortices, *Surv. Geophys.*, 2001, vol. 22, no. 3, pp. 179–263.
6. Carton, X., Oceanic Vortices, in *Fronts, Waves and Vortices in Geophysical Flows*, J. B. Flor (Ed.), Lect. Notes Phys., vol. 805, Berlin: Springer, 2010, pp. 61–108.
7. Carton, X., Morvan, M., Reinaud, J. N., Sokolovskiy, M. A., L'Hégaret, P., and Vic, C., Vortex Merger near a Topographic Slope in a Homogeneous Rotating Fluid, *Regul. Chaotic Dyn.*, 2017, vol. 22, no. 5, pp. 455–478.
8. Chelton, D. B., Schlax, M. G., Samelson, R. M., and de Szoeke, R. A., Global Observations of Large Oceanic Eddies, *Geophys. Res. Lett.*, 2007, vol. 34, no. 15, L15606, 5 pp.
9. Dritschel, D. G., A General Theory for Two-Dimensional Vortex Interactions, *J. Fluid Mech.*, 1995, vol. 293, pp. 269–303.
10. Dritschel, D. G., Vortex Merger in Rotating Stratified Flows, *J. Fluid Mech.*, 2002, vol. 455, pp. 83–101.
11. Koshel, K. V. and Ryzhov, E. A., Parametric Resonance with a Point-Vortex Pair in a Nonstationary Deformation Flow, *Phys. Lett. A*, 2012, vol. 376, no. 5, pp. 744–747.
12. Koshel, K. V., Reinaud, J. N., Riccardi, G., and Ryzhov, E. A., Entrapping of a Vortex Pair Interacting with a Fixed Point Vortex Revisited: 1. Point Vortices, *Phys. Fluids*, 2018, vol. 30, no. 9, 096603, 22 pp.
13. Koshel, K. V., Ryzhov, E. A., and Carton, X. J., Vortex Interactions Subjected to Deformation Flows: A Review, *Fluids*, 2019, vol. 4, no. 1, Art. 14, 48 pp.
14. Newton, P. K., Point Vortex Dynamics in the Post-Aref Era, *Fluid Dynam. Res.*, 2014, vol. 46, no. 3, 031401, 11 pp.
15. Perrot, X. and Carton, X., Point-Vortex Interaction in an Oscillatory Deformation Field: Hamiltonian Dynamics, Harmonic Resonance and Transition to Chaos, *Discrete Contin. Dyn. Syst. Ser. B*, 2009, vol. 11, no. 4, pp. 971–995.
16. Perrot, X. and Carton, X., 2D Vortex Interaction in Anon-Uniform Flow, *Theor. Comput. Fluid Dyn.*, 2010, vol. 24, no. 1, pp. 95–100.
17. Plotka, H. and Dritschel, D. G., Quasi-Geostrophic Shallow-Water Doubly-Connected Vortex Equilibria and Their Stability, *J. Fluid Mech.*, 2013, vol. 723, pp. 40–68.
18. Reinaud, J. N. and Dritschel, D. G., The Merger of Vertically Offset Quasi-Geostrophic Vortices, *J. Fluid Mech.*, 2002, vol. 469, pp. 287–315.

19. Reinaud, J.N. and Dritschel, D.G., The Critical Merger Distance between Two Co-Rotating Quasi-Geostrophic Vortices, *J. Fluid Mech.*, 2005, vol. 522, pp. 357–381.
20. Reinaud, J.N. and Carton, X., The Stability and the Nonlinear Evolution of Quasi-Geostrophic Hetons, *J. Fluid Mech.*, 2009, vol. 636, pp. 109–135.
21. Renault, L., McWilliams, J.C., and Gula, J., Dampening of Submesoscale Currents by Air-Sea Stress Coupling in the Californian Upwelling System, *Sci. Rep.*, 2018, vol. 8, 13388, 8 pp.
22. Renault, L., Marchesiello, P., Masson, S., and McWilliams, J.C., Remarkable Control of Western Boundary Currents by *Eddy Killing*, a Mechanical Air-Sea Coupling Process, *Geophys. Res. Lett.*, 2019, vol. 46, no. 5, pp. 2743–2751.
23. Sokolovskiy, M. A., Koshel, K. V., and Carton, X., Baroclinic Multipole Evolution in Shear and Strain, *Geophys. Astrophys. Fluid Dyn.*, 2011, vol. 105, nos. 4–5, pp. 506–535.
24. Sokolovskiy, M. A. and Verron, J., Finite-Core Hetons: Stability and Interactions, *J. Fluid Mech.*, 2000, vol. 423, pp. 127–154.
25. Sokolovskiy, M. A., Carton, X. J., and Filyushkin, B. N., Mathematical Modeling of Vortex Interaction Using a Three-Layer Quasigeostrophic Model: Part 1. Point-Vortex Approach, *Mathematics*, 2020, vol. 8, no. 8, Art. 1228, 13 pp.